

Optomechanical multimode Hamiltonian for nanophotonic waveguides

Hashem Zoubi* and Klemens Hammerer

*Institute for Theoretical Physics, Institute for Gravitational Physics (Albert Einstein Institute),**Leibniz University Hannover, Callinstrasse 38, 30167 Hannover, Germany*

(Received 3 August 2016; published 15 November 2016)

We develop a systematic method for deriving a quantum optical multimode Hamiltonian for the interaction of photons and phonons in nanophotonic dielectric materials by applying perturbation theory to the electromagnetic Hamiltonian. The Hamiltonian covers radiation pressure and electrostrictive interactions on equal footing. As a paradigmatic example, we apply our method to a cylindrical nanoscale waveguide and derive a Hamiltonian description of Brillouin quantum optomechanics. We show analytically that in nanoscale waveguides radiation pressure dominates over electrostriction, in agreement with recent experiments. The calculated photon-phonon coupling parameters are used to infer gain parameters of Stokes-Brillouin scattering in good agreement with experimental observations.

DOI: [10.1103/PhysRevA.94.053827](https://doi.org/10.1103/PhysRevA.94.053827)**I. INTRODUCTION**

Quantum optomechanics is the study of phenomena originating from the mutual interaction between electromagnetic radiation and mechanical motion [1–4]. In cavity optomechanics both the electromagnetic field and the mechanical vibrations are effectively restricted to single modes, and the strong coupling among phonons and photons achievable there enabled the demonstration of various quantum mechanical effects in recent years [5]. In the domain of optical frequencies, the strongest optomechanical coupling has been obtained in optomechanical crystals [6,7], where nanostructuring of dielectric materials is exploited to generate phonon and photon modes with strong spatial localization in order to enhance the light-matter interactions.

Very recently, experimental progress with nanophotonic waveguides supporting long-lived, high-frequency phonon modes evidenced that quantum optomechanical effects may become accessible also within a multimode version of optomechanics involving continua of propagating phonon and photon modes [8–13]. At the classical level, the Brillouin physics of interacting photons and phonons in waveguides has been studied extensively and led to the demonstration of a wide scope of nonlinear optical phenomena; see Refs. [14–17] for reviews. So far, the dominant mechanism for optomechanical coupling in waveguides has been electrostriction, that is the modulation of the index of refraction of the bulk dielectric material associated with its acoustic vibrations causing scattering of photons on these periodic index modulations. The recent experiments with nanophotonic waveguides entered a new regime where radiation pressure effects due to vibrational surface deformations start to dominate over electrostriction, which may result in vastly enhanced photon-phonon coupling. At the same time, these devices can maintain large quality factors for GHz mechanical modes extending over long cm-scale nanowires providing large optomechanical interactions over significant time and length scales. Overall, these developments indicate Brillouin quantum optomechanics as a promising

route toward integrable, broad-band platforms supporting strongly interacting fields of phonons and photons.

On the theoretical side, the description of Brillouin optomechanics in classical terms is well established [9,18–20]. A corresponding quantum mechanical description of electrostrictive coupling in terms of a multimode Hamiltonian has recently been derived by Agrawal *et al.* [21] in the context of multimode phonon cooling. In cavity quantum optomechanics involving single phonon and photon modes both effects are commonly taken into account [6,7] based on a formula by Johnson *et al.* [22]. Progress toward extending the cavity optomechanical description to the regime of Brillouin optomechanics has been achieved by Van Laer *et al.* [23] by relating Brillouin gain parameters to the optomechanical single-photon coupling strengths. Sipe *et al.* [24] very recently provided a Hamiltonian treatment of stimulated Brillouin scattering in nanoscale integrated waveguides accounting for electrostriction and radiation pressure, following the method of Refs. [20,22].

In the present work we aim to contribute to this development of a quantum theory of Brillouin optomechanics in two respects: First, we derive the multimode Hamiltonian for Brillouin optomechanics by applying perturbation theory directly to the field Hamiltonian for the case of an isotropic dielectric material, which includes on equal footing electrostriction and radiation pressure mechanisms. Our derivation reproduces the results of Sipe *et al.* [24] but avoids the rather technical smoothing procedures introduced by Johnson *et al.* [22], employed also in Ref. [24], in order to deal with discontinuities at surfaces. We believe that the point of view advocated in the present derivation provides valuable physical insight to an otherwise rather unintuitive result. Second, we apply the general formula of the multimode Hamiltonian for Brillouin optomechanics to the important special case of a cylindrical nanowaveguide, and evaluate analytically the parameters in the Hamiltonian characterizing the phonon-photon coupling strength. We use our analytical expressions to demonstrate the domination of radiation pressure effect over electrostriction for nanoscale waveguides, and determine optimal parameter regimes exhibiting maximal coupling. The formalism is applicable to systems of any dimensional scales, ranging from cavity optomechanical systems involving localized photon and

*hashem.zoubi@itp.uni-hannover.de

phonon modes up to bulk materials in which photons and phonons are described by continuous fields as in Brillouin optomechanics.

We treat a cylindrical nanoscale waveguide (tapered fiber), which exhibits a (quasi)continuum of modes propagating in the longitudinal direction with localized discrete modes due transverse confinement. We consider in much detail the case of a nanofiber made of silicon material that is embedded in free space. We analytically solve for the photon and phonon vector mode functions and dispersion relations and calculate the photon-phonon coupling parameters originating from electrostriction and radiation pressure mechanisms. This case is motivated by the recent progress in Brillouin optomechanics [10–13,25], but also by the work on tapered optical nanofibers that have been used in manipulating, trapping, and detecting neutral cold and ultracold atoms [26,27], in which optically active mechanical modes of tapered nanofibers have been also investigated [28]. Moreover, we provide a means to compare the theoretically calculated photon-phonon coupling parameter with the experimentally observed gain parameter. Moving to the real-space representation of the Hamiltonian, we solve the system of equations for the Stokes stimulated Brillouin scattering. The Stokes field is amplified with a gain parameter that is related to the photon-phonon coupling parameter in the derived Hamiltonian, similar to what has been discussed by Van Laer *et al.* [23].

The paper is organized as follows. Section II contains the derivation of the classical, perturbed Hamiltonians for the coupled light and mechanical excitations through radiation pressure and electrostriction mechanisms. The discussion is followed by the canonical quantization of the coupled classical fields, where the interacting multimode photon and phonon Hamiltonian is derived. The photon-phonon coupling parameters are explicitly calculated for the case of cylindrical nanowires in Sec. III. A relation between the photon-phonon coupling parameter and the gain parameter of Stokes stimulated Brillouin scattering is presented in Sec. IV, and the coupled photon-phonon real-space Hamiltonian is introduced. The appendices include the full solutions of the electromagnetic fields and the mechanical excitations in a cylindrical dielectric waveguide.

II. COUPLING AMONG ELECTROMAGNETIC FIELD AND MECHANICAL VIBRATIONS

We aim first to derive the classical Hamiltonian that represents the mutual influence of the mechanical excitations and the electromagnetic field in a bounded dielectric medium, and which are characterized by the electric field $\mathbf{E}(\mathbf{x})$ and the mechanical displacement field $\mathbf{Q}(\mathbf{x})$, respectively. The electromagnetic field in a dielectric, lossless, and nonmagnetic medium with a scalar permittivity $\epsilon(\mathbf{x})$ is described by the Hamiltonian [29]

$$H = \frac{1}{2} \int dV \left\{ \frac{1}{\epsilon(\mathbf{x})} |\mathbf{D}(\mathbf{x})|^2 + \frac{1}{\mu_0} |\mathbf{B}(\mathbf{x})|^2 \right\}, \quad (1)$$

where the electric displacement field is defined by $\mathbf{D}(\mathbf{x}) = \epsilon(\mathbf{x})\mathbf{E}(\mathbf{x})$. The Hamiltonian coupling of photons and phonons follows from evaluating the correction δH to H due to a mechanical displacement $\mathbf{Q}(\mathbf{x})$ causing a perturbation $\delta\epsilon(\mathbf{x})$

in the permittivity $\epsilon(\mathbf{x})$. We will consider corrections in first order of the mechanical displacement throughout the paper and limit the discussion to isotropic fluctuations in the dielectric constant. The explicit dependence of $\delta\epsilon(\mathbf{x})$ on $\mathbf{Q}(\mathbf{x})$ differs for radiation pressure and electrostrictive interaction, and will be detailed below. Nevertheless, both effects are covered by the perturbation to the field Hamiltonian in Eq. (1):

$$\delta H = \frac{1}{2} \int dV \delta\epsilon^{-1}(\mathbf{x}) |\mathbf{D}(\mathbf{x})|^2. \quad (2)$$

Here $\delta\epsilon^{-1}(\mathbf{x})$ in Eq. (2) denotes the perturbation of the inverse of the permittivity, which is not to be confused with the inverse of the perturbation $[\delta\epsilon(\mathbf{x})]^{-1}$. The contributions to δH due to the corrections in the amplitude of the electric displacement field \mathbf{D} are negligibly small, on the order of the ratio of phonon to photon frequency, as shown in Appendix A. A further correction of the same order is introduced through magnetic polarization effects [24]. Note that the perturbation of the field Hamiltonian Eq. (1) needs to be done in the representation where the energy density is expressed in terms of the electric displacement field. If instead the electric field \mathbf{E} is used, the contributions due to corrections of the field amplitude will be significant, cf. Appendix A, and δH would take a much more cumbersome form.

We consider a dielectric material with permittivity $\epsilon(\mathbf{x}) = \epsilon_1$ in a volume V_1 , which is localized in a surrounding medium with permittivity $\epsilon(\mathbf{x}) = \epsilon_2$ occupying the complementary volume V_2 . For a dielectric material in vacuum $\epsilon_2 = \epsilon_0$. The unperturbed permittivity can be written as

$$\epsilon(\mathbf{x}) = \epsilon_2 + (\epsilon_1 - \epsilon_2)\Theta(\mathbf{x}), \quad (3)$$

where $\Theta(\mathbf{x})$ is a step function defined by

$$\Theta(\mathbf{x}) = \begin{cases} 1 & \text{for } \mathbf{x} \in V_1 \\ 0 & \text{for } \mathbf{x} \in V_2 \end{cases}$$

A mechanical displacement $\mathbf{Q}(\mathbf{x})$ of the dielectric medium in V_1 will affect the material's permittivity in two ways: In the electrostrictive mechanism, the fluctuations change the magnitude of the permittivity of the material in V_1 at a fixed boundary. Radiation pressure in turn corresponds to fluctuations in the material boundary at a fixed magnitude of ϵ_1 . Thus, the perturbed permittivity can be written as

$$\epsilon(\mathbf{x}) = \epsilon_2 + [\epsilon_1(\mathbf{Q}) - \epsilon_2]\Theta(\mathbf{x} + \mathbf{Q}),$$

where $\epsilon_1(\mathbf{Q})|_{\mathbf{Q}=0} = \epsilon_1$. The first-order corrections is $\delta\epsilon(\mathbf{x}) = \delta\epsilon_{\text{rp}}(\mathbf{x}) + \delta\epsilon_{\text{el}}(\mathbf{x})$ and the contributions from radiation pressure and electrostriction are, respectively,

$$\delta\epsilon_{\text{rp}}(\mathbf{x}) = (\epsilon_1 - \epsilon_2)\mathbf{Q}(\mathbf{x}) \cdot \nabla\Theta(\mathbf{x}), \quad (4)$$

$$\delta\epsilon_{\text{el}}(\mathbf{x}) = \delta\epsilon_1(\mathbf{Q})\Theta(\mathbf{x}). \quad (5)$$

The contributions of these two perturbations to the interaction Hamiltonian in Eq. (2) will be treated in the following two subsections.

A. Radiation pressure

We note first that $\nabla\Theta(\mathbf{x})$ in Eq. (4) denotes a δ distribution whose effect is to turn volume integrals into surface integrals

over the boundary ∂V between V_1 and V_2 , that is

$$\int_{V_1+V_2} dV \mathbf{f}(\mathbf{x}) \cdot \nabla \Theta(\mathbf{x}) = \int_{\partial V} d\mathbf{A} \cdot \mathbf{f}(\mathbf{x}), \quad (6)$$

where $d\mathbf{A}$ is the infinitesimal surface element. Thus, when using Eq. (4) in Eq. (2) it will be vital to take care that the remaining integrand does not contain discontinuities on the boundary surface rendering the integral undefined.

This concerns in particular the discontinuity in the field component of $\mathbf{D}(\mathbf{x})$ parallel to the boundary surface. In order to overcome this difficulty we consider an (arbitrarily thin) shell volume V' enclosing the boundary surface ∂V , and rewrite the contribution to the interaction Hamiltonian Eq. (2) within V' in terms of the fields $\mathbf{E}_{\parallel}(\mathbf{x}) = \mathbf{D}_{\parallel}(\mathbf{x})/\epsilon(\mathbf{x})$ and $\mathbf{D}_{\perp}(\mathbf{x})$ parallel and orthogonal to the surface that are both continuous,

$$\delta H = \frac{1}{2} \int_{V'} dV \{-\delta\epsilon(\mathbf{x})|\mathbf{E}_{\parallel}(\mathbf{x})|^2 + \delta\epsilon^{-1}(\mathbf{x})|\mathbf{D}_{\perp}(\mathbf{x})|^2\}. \quad (7)$$

Here we used $\epsilon^2(\mathbf{x})\delta\epsilon^{-1}(\mathbf{x}) = -\delta\epsilon(\mathbf{x})$. In restricting the integration to the shell volume V' we anticipate, in view of Eq. (6), that it is the energy within this subvolume that will be relevant for the perturbation due to radiation pressure. The remaining hurdle is to arrive at a well-behaved perturbation of the inverse permittivity in Eq. (7). This can be achieved by expressing the inverse as $\epsilon^{-1}(\mathbf{x}) = \epsilon_2^{-1} + (\epsilon_1^{-1} - \epsilon_2^{-1})\Theta(\mathbf{x})$, which yields

$$\delta\epsilon_{\text{rp}}^{-1}(\mathbf{x}) = (\epsilon_1^{-1} - \epsilon_2^{-1})\mathbf{Q}(\mathbf{x}) \cdot \nabla\Theta(\mathbf{x}), \quad (8)$$

for the contribution due to radiation pressure.

Finally, we can use Eqs. (4), (6), and (8) in Eq. (7) to arrive at the Hamiltonian describing radiation pressure interaction

$$\begin{aligned} \delta H_{\text{rp}} = & -\frac{1}{2} \int_{\partial V} d\mathbf{A} \cdot \mathbf{Q}(\mathbf{x}) \\ & \times \{\Delta\epsilon|\mathbf{E}_{\parallel}(\mathbf{x})|^2 - \Delta(\epsilon^{-1})|\mathbf{D}_{\perp}(\mathbf{x})|^2\}. \end{aligned} \quad (9)$$

We used the symbols $\Delta\epsilon = \epsilon_1 - \epsilon_2$ and $\Delta(\epsilon^{-1}) = \epsilon_1^{-1} - \epsilon_2^{-1}$ following the notation introduced by Johnson *et al.* in Ref. [22]. The integral in Eq. (9) is over the surface ∂V of the dielectric medium, and all fields are evaluated on that surface. Thanks to the continuity of \mathbf{E}_{\parallel} and \mathbf{D}_{\perp} there is no ambiguity in evaluating the field on either side of the surface.

The result presented here agrees with the one derived in Ref. [22] for the perturbed eigenfrequency of photonic field modes. Johnson *et al.* used a smoothing procedure in order to deal with the difficulty of discontinuities of field amplitudes at the surface. The alternative approach presented here avoids such technicalities and at the same time provides directly the interaction Hamiltonian covering both frequency shifts of photon modes and Brillouin scattering among different field modes. It is this last aspect that is of main interest in the description of the optomechanics of extended nanophotonic waveguides. Furthermore, the interaction Hamiltonian Eq. (9) is directly amenable to quantization, as will be done in Sec. II C, and provides firm grounds for the description of radiation pressure effects in Brillouin quantum optomechanics.

B. Electrostriction

Electrostriction appears due to the tendency of a dielectric material to be compressed in the presence of light, and as

a consequence to excite mechanical vibrations in the medium [18,19]. The appearance of mechanical vibrations modulate the optical properties and result in small changes in the dielectric constant that induce scattering of the light. A Hamiltonian description of electrostriction has been derived previously by Agrawal *et al.* [21]. For completeness we present a derivation within the present approach, starting from Eq. (12) for the perturbation of the bulk value of the permittivity due to a mechanical displacement.

By means of the electrostriction constant γ_{el} the change in the permittivity can be related to fluctuations of the mass density ρ ,

$$\delta\epsilon_1(\mathbf{Q}) = \epsilon_0 \frac{\gamma_{\text{el}}}{\rho} \delta\rho(\mathbf{Q}), \quad (10)$$

which in turn is determined through the mechanical displacement,

$$\delta\rho(\mathbf{Q}) \simeq -\rho \nabla \cdot \mathbf{Q}(\mathbf{x}). \quad (11)$$

Overall, we arrive from Eq. (12) at

$$\delta\epsilon_{\text{el}}(\mathbf{x}) = -\epsilon_0 \gamma_{\text{el}} [\nabla \cdot \mathbf{Q}(\mathbf{x})] \Theta(\mathbf{x}). \quad (12)$$

Electrostriction mechanism in nanoscale structures can give rise to anisotropic phenomena. Anisotropic contributions induced by longitudinal phonons in nanoscale waveguides are immaterial [30]. As we concentrate mainly in processes involving longitudinal phonons we treat here only the isotropic case of scalar fluctuations [18,19]. Anisotropic phenomena induced by tensor fluctuations of the dielectric function are beyond the scope of the present paper.

The relation Eq. (12) can be used directly in Eq. (2) when resorting to the representation of δH in terms of the electric field (using again $\epsilon^2(\mathbf{x})\delta[\epsilon^{-1}(\mathbf{x})] = -\delta\epsilon(\mathbf{x})$),

$$\delta H_{\text{el}} = -\frac{1}{2} \int_{V_1+V_2} dV \delta\epsilon_{\text{el}}(\mathbf{x}) |\mathbf{E}(\mathbf{x})|^2. \quad (13)$$

No issues regarding discontinuities in the integrand arise here since the domain of integration is effectively limited to the volume V_1 occupied by the dielectric due to the step function in Eq. (12). Here δH_{el} decreases by increasing $\delta\epsilon$ as expected. Finally, this yields the Hamiltonian for the electrostrictive interaction of photons and phonons,

$$\delta H_{\text{el}} = \gamma_{\text{el}} \frac{\epsilon_0}{2} \int_{V_1} dV [\nabla \cdot \mathbf{Q}(\mathbf{x})] |\mathbf{E}(\mathbf{x})|^2. \quad (14)$$

It is evident from Eqs. (9) and (14) that radiation pressure and electrostriction are surface and volume effects, respectively. For sufficiently small dimensions radiation pressure will therefore dominate and may ultimately provide largely enhanced coupling strengths per single photon and phonon. We will show this explicitly for the example of a cylindrical waveguide in Sec. III. Before that, we will quantize the interaction Hamiltonians in Eqs. (9) and (14), and extract the quantum mechanical coupling strengths at the single photon/phonon level.

C. Quantization

We aim to derive the photon-phonon interaction Hamiltonian in dielectric media by canonically quantizing the

electromagnetic and mechanical fields that were presented in the previous sections [29,31–33]. The Hamiltonian of the free photon field reads

$$\hat{H}_{\text{phot}} = \sum_{\alpha} \hbar \omega_{\alpha} \hat{a}_{\alpha}^{\dagger} \hat{a}_{\alpha}, \quad (15)$$

where the summation is over all the photon modes and the summation index α comprises any index labeling photon modes for a given geometry. In the following we will assume a discrete set of indices, such that $\hat{a}_{\alpha}^{\dagger}$ and \hat{a}_{α} are dimensionless bosonic creation and annihilation operators, and fulfill $[\hat{a}_{\alpha}, \hat{a}_{\beta}^{\dagger}] = \delta_{\alpha\beta}$. Continuous index sets as relevant to problems with, e.g., translational symmetry can be attained via appropriate limiting procedures, as detailed, for example, in Ref. [34]. The electric field operator reads $\hat{\mathbf{E}}(\mathbf{x}) = \hat{\mathbf{E}}^{(+)}(\mathbf{x}) + \hat{\mathbf{E}}^{(-)}(\mathbf{x})$, where

$$\hat{\mathbf{E}}^{(+)}(\mathbf{r}, t) = i \sum_{\alpha} \mathcal{E}_{\alpha} \hat{a}_{\alpha} \mathbf{U}_{\alpha}(\mathbf{x}), \quad (16)$$

and $\hat{\mathbf{E}}^{(-)} = (\hat{\mathbf{E}}^{(+)})^{\dagger}$. The (dimensionless) vector function $\mathbf{U}_{\alpha}(\mathbf{x})$ of mode α and the eigenfrequency ω_{α} are obtained by solving Maxwell's equations with appropriate boundary conditions, cf. Appendix A. The electric field amplitude of a single photon in mode α is

$$\mathcal{E}_{\alpha} = \sqrt{\frac{\hbar \omega_{\alpha}}{2\epsilon_0 V_{\alpha}^{\text{phot}}}}. \quad (17)$$

The effective volume V_{α}^{phot} is calculated from the normalization condition,

$$\int dV |\mathbf{U}_{\alpha}(\mathbf{x})|^2 = V_{\alpha}^{\text{phot}}. \quad (18)$$

On the other hand, the phonon Hamiltonian reads

$$\hat{H}_{\text{phon}} = \sum_{\nu} \hbar \Omega_{\nu} \hat{b}_{\nu}^{\dagger} \hat{b}_{\nu}, \quad (19)$$

where \hat{b}_{ν}^{\dagger} and \hat{b}_{ν} are the bosonic creation and annihilation operators of a phonon in mode ν with angular frequency Ω_{ν} . The index ν again stands for any discrete index relevant for a given geometry. The operator corresponding to the mechanical displacement field is $\hat{\mathbf{Q}}(\mathbf{x}) = \hat{\mathbf{Q}}^{(+)}(\mathbf{x}) + \hat{\mathbf{Q}}^{(-)}(\mathbf{x})$, where

$$\hat{\mathbf{Q}}^{(+)}(\mathbf{x}) = \sum_{\nu} Z_{\nu} \hat{b}_{\nu} \mathbf{W}_{\nu}(\mathbf{x}), \quad (20)$$

and $\hat{\mathbf{Q}}^{(-)} = (\hat{\mathbf{Q}}^{(+)})^{\dagger}$. Here $\mathbf{W}_{\nu}(\mathbf{x})$ is the (dimensionless) vector mode function of phonons with eigenfrequency Ω_{ν} , which is obtained by solving the equations of motion of mechanical excitation as shown in Sec. III. The zero-point-fluctuation of mode ν is

$$Z_{\nu} = \sqrt{\frac{\hbar}{2M_{\nu}^{\text{phon}} \Omega_{\nu}}}. \quad (21)$$

The effective mass associated to phonon mode ν is given by $M_{\nu}^{\text{phon}} = \rho V_{\nu}^{\text{phon}}$, where ρ is the medium's mass density and V_{ν}^{phon} is the phonon effective volume, which can be calculated

from the normalization condition,

$$\int dV |\mathbf{W}_{\nu}(\mathbf{x})|^2 = V_{\nu}^{\text{phon}}. \quad (22)$$

The quantized interaction Hamiltonian is obtained from the classical one by replacing the displacement and the electromagnetic fields by operators and using normal ordering. We will use the notation $(:\hat{X}:)$ to denote the normally ordered form of the operator \hat{X} . The radiation pressure Hamiltonian reads

$$\hat{H}_{\text{rp}} = -\frac{1}{2} \int_{\partial V} :d\mathbf{A} \cdot \hat{\mathbf{Q}}(\mathbf{x}) \times \{\Delta \epsilon |\hat{\mathbf{E}}_{\parallel}(\mathbf{x})|^2 - \Delta(\epsilon^{-1}) |\hat{\mathbf{D}}_{\perp}(\mathbf{x})|^2\}, \quad (23)$$

and the electrostriction Hamiltonian reads

$$\hat{H}_{\text{el}} = \gamma_{\text{el}} \frac{\epsilon_0}{2} \int_{V_1} dV :(\nabla \cdot \hat{\mathbf{Q}}(\mathbf{x})) |\hat{\mathbf{E}}(\mathbf{x})|^2:. \quad (24)$$

In terms of creation and annihilation operators, using the above definitions, the interaction Hamiltonian is

$$\begin{aligned} \hat{H}_I &= \hat{H}_{\text{rp}} + \hat{H}_{\text{el}} \\ &= \hbar \sum_{\alpha\alpha'\nu} \{f_{\alpha\alpha'\nu}^* \hat{b}_{\nu}^{\dagger} \hat{a}_{\alpha}^{\dagger} \hat{a}_{\alpha} + f_{\alpha\alpha'\nu} \hat{a}_{\alpha}^{\dagger} \hat{a}_{\alpha'} \hat{b}_{\nu}\}. \end{aligned} \quad (25)$$

Thus, the optomechanical photon-phonon coupling strength (of dimension Hz) is $f_{\alpha\alpha'\nu} = f_{\alpha\alpha'\nu}^{\text{rp}} + f_{\alpha\alpha'\nu}^{\text{el}}$, where the radiation pressure coupling is given by

$$\begin{aligned} f_{\alpha\alpha'\nu}^{\text{rp}} &= -\frac{1}{2} Z_{\nu} \mathcal{E}_{\alpha} \mathcal{E}_{\alpha'} \int_{\partial V} d\mathbf{A} \cdot \mathbf{W}_{\nu}(\mathbf{x}) \\ &\times \{\Delta \epsilon \mathbf{U}_{\alpha}^{\parallel*}(\mathbf{x}) \cdot \mathbf{U}_{\alpha'}^{\parallel}(\mathbf{x}) - \epsilon_1^2 \Delta(\epsilon^{-1}) \\ &\times \mathbf{U}_{\alpha}^{\perp<*}(\mathbf{x}) \cdot \mathbf{U}_{\alpha'}^{\perp<}(\mathbf{x})\}. \end{aligned} \quad (26)$$

All mode functions are evaluated on the boundary surface, and most important here is that the perpendicular components, $\mathbf{U}_{\alpha}^{\perp<}$, are evaluated on the internal side of the surface, as indicated by the superscript symbol ($<$). For the electrostrictive coupling we get

$$f_{\alpha\alpha'\nu}^{\text{el}} = \gamma_{\text{el}} \frac{\epsilon_0}{2} Z_{\nu} \mathcal{E}_{\alpha} \mathcal{E}_{\alpha'} \int_{V_1} dV [\nabla \cdot \mathbf{W}_{\nu}(\mathbf{x})] \mathbf{U}_{\alpha}^*(\mathbf{x}) \cdot \mathbf{U}_{\alpha'}(\mathbf{x}). \quad (27)$$

The results are applicable to any dielectric material ranging from fully confined media, as for a resonator, up to partly confined media, as for a waveguide. The interactions are consistent with the results in Ref. [24], but here we give explicitly the appropriate normalized amplitudes.

III. COUPLING AMONG PHOTONS AND PHONONS IN NANOPHOTONIC WAVEGUIDES

The formalism of the previous section has been applied extremely successfully to quantum optomechanical systems comprising single electromagnetic and mechanical modes. Our main concern here is the application to extended media,

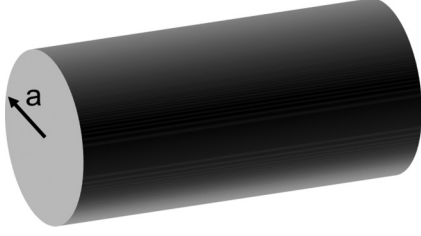


FIG. 1. An optical nanofiber of radius a and refractive index n , which is localized in free space.

where the multimode character of the interaction Hamiltonian is essential but at the same time field confinement due to small spatial extensions yields strong coupling due to enhanced radiation pressure. In the following we present analytical results for the coupling strengths $f_{\alpha\alpha'\nu}^{\text{IP}}$ and $f_{\alpha\alpha'\nu}^{\text{el}}$ for the most elementary such geometry, namely a cylindrical nanophotonic waveguide. We consider a dielectric nanowire that is localized in free space and extended along the z direction over a length L with a nanoscale radius a , as seen in Fig. 1. The dielectric constants are $\epsilon_1 = \epsilon_0 n^2$ and $\epsilon_2 = \epsilon_0$, where n is the medium refractive index. Recently, such tapered optical nanofibers have been intensively studied [26–28].

The strong confinement in the transverse direction results in discrete modes for both the electromagnetic and mechanical fields. In the following we will consider only a single transverse mode for the photons and phonons. The electromagnetic and mechanical fields can propagate along the waveguide axis with wave number k , which takes on the values $k = \frac{2\pi}{L}m$ with $m = 0, \pm 1, \pm 2, \dots$, where L is the waveguide length and we use periodic boundary conditions. Phonon wave numbers will be denoted by q and have a natural cutoff that is given by the inverse of the crystal lattice constant.

A. Photons in nanoscale waveguides

The photon Hamiltonian for a single transverse mode reads

$$\hat{H}_{\text{phot}} = \sum_k \hbar\omega_k \hat{a}_k^\dagger \hat{a}_k, \quad (28)$$

where \hat{a}_k^\dagger and \hat{a}_k are the creation and annihilation operators of a photon of wave number k and angular frequency ω_k . The electric field operator reads, in cylindrical coordinates,

$$\hat{\mathbf{E}}(r, \theta, z) = i \sum_k \sqrt{\frac{\hbar\omega_k}{2\epsilon_0 V_k^{\text{phot}}}} \times \{\hat{a}_k \mathbf{u}_k(r, \theta) e^{ikz} - \hat{a}_k^\dagger \mathbf{u}_k^*(r, \theta) e^{-ikz}\}, \quad (29)$$

where $\mathbf{u}_k(r, \theta)$ is the transverse vector mode function, and the effective mode volume V_k^{phot} is defined by $\int dV |\mathbf{u}_k(r, \theta)|^2 = V_k^{\text{phot}}$.

The lowest propagating mode in an optical nanofiber is the HE_{11} mode. We concentrate in photons with a fixed polarization, and we consider rotating polarization with left- or right-hand circular rotations. Detailed calculations of the cylindrical waveguide photon dispersions and mode functions are given in Appendix B. The photon dispersion, which is the relation between the angular frequency, ω , and the wave

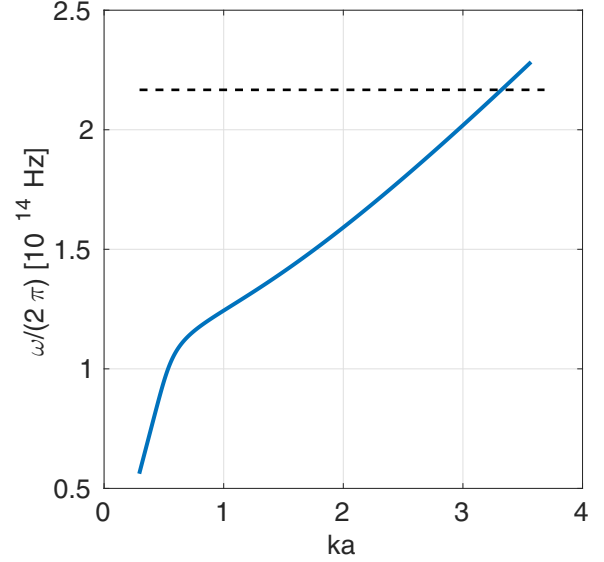


FIG. 2. The lowest HE_{11} fiber mode is presented as $\omega/(2\pi)$ vs. ka . Here $n = 3.5$ for silicon material. Beyond the dashed line at $\omega/(2\pi) \approx 2.186 \times 10^{14}$ Hz other photon branches start to appear.

number along the fiber axis, k , can be extracted from the expression [35]

$$\frac{J_0(pa)}{paJ_1(pa)} = \left(\frac{1+n^2}{2n^2}\right) \frac{K_0(qa) + K_2(qa)}{2qaK_1(qa)} + \frac{1}{p^2a^2} - \left\{ \left(\frac{n^2-1}{2n^2}\right)^2 \left(\frac{K_0(qa) + K_2(qa)}{2qaK_1(qa)}\right)^2 + \left(\frac{k}{nk_0}\right)^2 \left(\frac{1}{q^2a^2} + \frac{1}{p^2a^2}\right)^2 \right\}^{1/2}, \quad (30)$$

where $p = \sqrt{k_0^2 n^2 - k^2}$, and $q = \sqrt{k^2 - k_0^2}$, with $k_0 = \omega/c$. Propagating modes can appear only in the range $1 \leq \frac{k}{k_0} \leq n$. In the literature this result is commonly represented in terms of the fundamental parameter $V = k_0 a \sqrt{n^2 - 1}$. For silicon we have $n \approx 3.5$ and up to about $V \approx 3.84$ only the HE_{11} photons propagate in the fiber, and beyond $V \approx 3.84$ TM and TE modes can be excited. The HE_{11} dispersion relation is plotted in Fig. 2 for $\omega/(2\pi)$ as a function of ka . For small wave numbers the photons are unconfined in the nanofiber and propagate with the group velocity c/n , but beyond $ka \approx 0.7$ they get confined and propagate with almost linear dispersion of group velocity $v_g \approx c/5$.

The vector mode functions inside the fiber, that is for $(r < a)$, are given by

$$\begin{aligned} u_k^{r<} &= -iB \frac{k}{2p} [(1-s)J_0(pr) - (1+s)J_2(pr)] e^{\pm i\theta}, \\ u_k^{\theta<} &= \pm B \frac{k}{2p} [(1-s)J_0(pr) + (1+s)J_2(pr)] e^{\pm i\theta}, \\ u_k^{z<} &= B J_1(pr) e^{\pm i\theta}, \end{aligned} \quad (31)$$

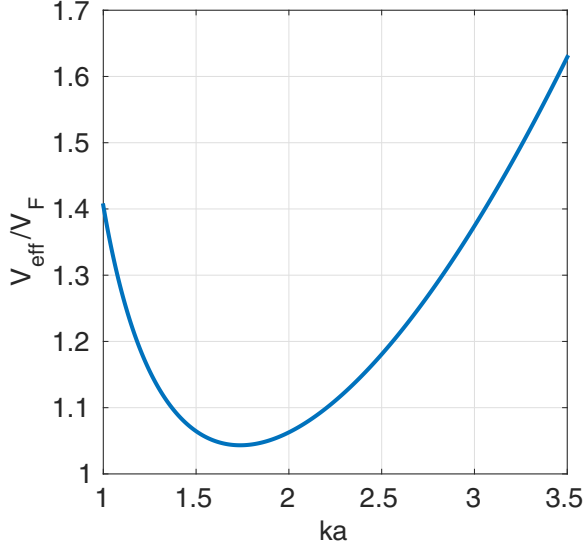


FIG. 3. The relative photon mode volume V_k^{phot}/V_F vs. ka for HE_{11} fiber photons.

and outside the fiber, that is ($r > a$), are given by

$$\begin{aligned} u_k^{r>} &= -iB \frac{k}{2q} \frac{J_1(pa)}{K_1(qa)} \\ &\quad [(1-s)K_0(qr) + (1+s)K_2(qr)]e^{\pm i\theta}, \\ u_k^{\theta>} &= \pm B \frac{k}{2q} \frac{J_1(pa)}{K_1(qa)} \\ &\quad [(1-s)K_0(qr) - (1+s)K_2(qr)]e^{\pm i\theta}, \\ u_k^{z>} &= B \frac{J_1(pa)}{K_1(qa)} K_1(qr)e^{\pm i\theta}, \end{aligned} \quad (32)$$

where

$$s = \left[\frac{1}{p^2 a^2} + \frac{1}{q^2 a^2} \right] \left\{ \frac{J_1'(pa)}{pa J_1(pa)} + \frac{K_1'(qa)}{qa K_1(qa)} \right\}^{-1}, \quad (33)$$

and $(\pm\theta)$ stand for left- and right-hand circular polarizations. The parameter B is fixed from the normalization relation stated above. In Fig. 3 we plot the effective volume V_k^{phot} of photon mode k relative to the total fiber volume $V_F = \pi a^2 L$ as a function of ka . Here a minimum appears around $ka \approx 1.74$ in which the photon mode is highly concentrated inside the fiber, and a small part penetrates outside. For example, for $a = 250$ nm we get a minimum at $\lambda \approx 900$ nm.

B. Phonons in nanoscale waveguides

The phonon Hamiltonian for a single mode is given by

$$\hat{H}_{\text{phon}} = \sum_q \hbar \Omega_q \hat{b}_q^\dagger \hat{b}_q, \quad (34)$$

where \hat{b}_q^\dagger and \hat{b}_q are the creation and annihilation operators of a phonon of wave number q and angular frequency Ω_q . The

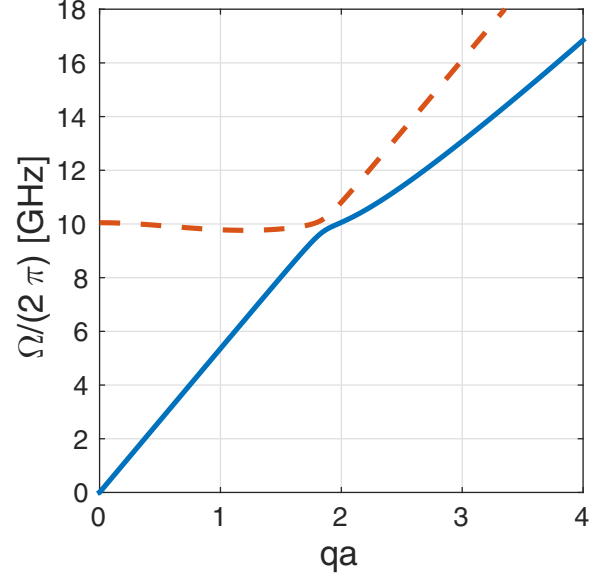


FIG. 4. The lowest two branches of the longitudinal phonon modes, for $\Omega/(2\pi)$ vs. qa for a silicon waveguide ($n = 3.5$): Lower, acoustic branch (solid blue line); upper, vibrational branch (dashed red line).

displacement operator is defined by

$$\hat{\mathbf{Q}}(r, \theta, z) = \sum_q Z_q \{ \hat{b}_q \mathbf{w}_q(r, \theta) e^{iqz} + \hat{b}_q^\dagger \mathbf{w}_q^*(r, \theta) e^{-iqz} \}, \quad (35)$$

where $\mathbf{w}_q(r, \theta)$ is the transverse vector mode function. The zero-point-fluctuation is $Z_q = (\hbar/2M_q \Omega_q)^{1/2}$ with effective mass $M_q = \rho V_q^{\text{phon}}$ and effective phonon mode volume $\int dV |\mathbf{w}_q(r, \theta)|^2 = V_q^{\text{phon}}$.

In optical nanofibers torsional, longitudinal, and flexural phonons can be excited. Here we consider only longitudinal modes, as the torsional modes decouple to the light through radiation pressure and the flexural modes are of higher energy. Detailed calculations of the cylindrical waveguide phonon dispersions and mode functions are given in Appendix C. The longitudinal phonon dispersion can be extracted from the expression [36]

$$(q^2 - \eta_l^2)^2 \frac{\eta_l a J_0(\eta_l a)}{J_1(\eta_l a)} + 4q^2 \eta_l^2 \frac{\eta_l a J_0(\eta_l a)}{J_1(\eta_l a)} = 2\eta_l^2 (q^2 + \eta_l^2), \quad (36)$$

where we have $\eta_l^2 = \frac{\Omega_l^2}{v_l^2} - q^2$, and $\eta_t^2 = \frac{\Omega_t^2}{v_t^2} - q^2$. The lowest two longitudinal branches are plotted in Fig. 4 for $\Omega/(2\pi)$ as a function of qa . We treat silicon material with $v_l = 8433$ m/s and $v_t = 5843$ m/s. For small wave numbers $qa \ll 1$, the lowest acoustic modes have a linear dispersion, and the lowest vibrational modes are almost dispersion-less up to $ka \approx 2$. Both branches become linear beyond the anticrossing point.

The vector mode functions are given by

$$\begin{aligned} w_q^r &= -A \eta_l J_1(\eta_l r) + i C q J_1(\eta_l r), \\ w_q^\theta &= 0, \\ w_q^z &= i A q J_0(\eta_l r) - C \eta_l J_0(\eta_l r). \end{aligned} \quad (37)$$

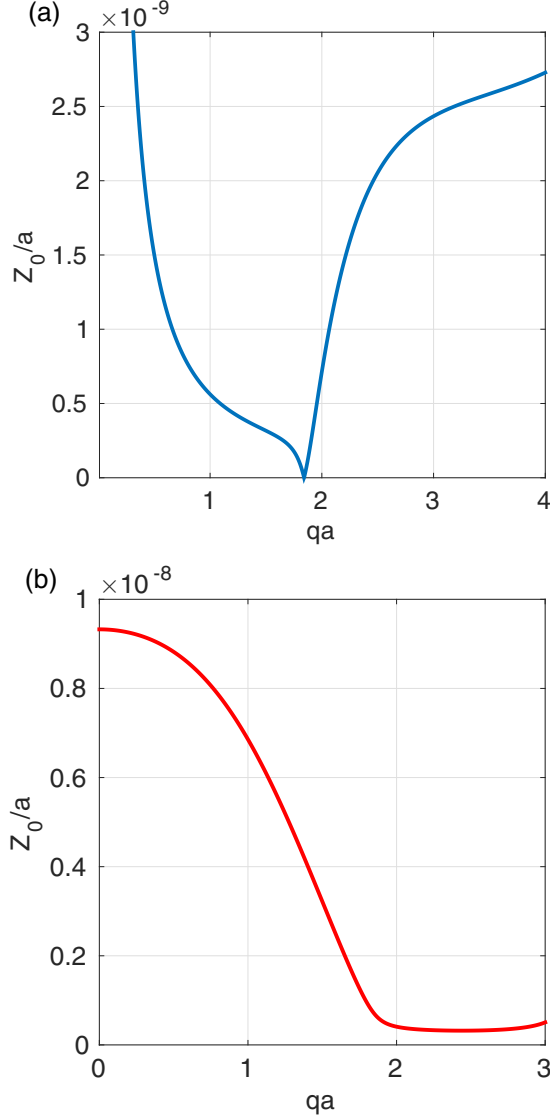


FIG. 5. The relative zero-point fluctuation, Z_q/a vs. qa , (a) for acoustic modes, and (b) for vibrational modes.

The parameters A and C are fixed using the boundary condition relation,

$$C = \frac{2iq\eta_l}{[\eta_l^2 - q^2]} \frac{J_1(\eta_l a)}{J_1(\eta_l a)} A, \quad (38)$$

and the normalization relation stated above. Note that A also plays the role of a scaling factor that takes care of the appropriate units.

For illustration we consider a nanofiber of radius $a = 250$ nm and length $L = 1$ cm made of silicon material (density $\rho = 2328$ kg/m³). In Figs. 5(a) and 5(b) we plot the zero-point-fluctuation relative to the fiber radius, Z_q/a , as a function of qa , for the lowest two branches. It appears that the zero-point fluctuations decrease with increasing qa for the acoustic modes, where a singularity appears around $qa \approx 1.8$, and increase afterward for larger qa . The singularity appears at the anticrossing point among the acoustic and the lowest vibrational modes, as seen in Fig. 4. The vibrational

modes have finite zero-point-fluctuations that decrease with increasing qa .

Importantly, the phonon frequencies for both acoustic and vibrational modes are in the GHz regime, which allows to achieve low thermal occupation numbers at cryogenic temperatures. Moreover, mechanical quality factors measured in recent experiments with tapered nanofibers were in the range of 10^4 [28]. For square-shaped waveguides, mechanical quality factors of several 100 have been measured [12,13]. In view of the tremendous progress made regarding mechanical quality factors of single-mode optomechanical systems we expect that there is vast room for improvement here with optimized nanostructures.

C. Photon-phonon interactions

Insertingly, the analytical expressions for the nanowire photon and phonon modes derived in the previous sections into the general expression for the photon-phonon interaction Hamiltonian Eq. (25) yields

$$\hat{H}_I = \hbar \sum_{kq} \{f_{kq}^* \hat{b}_q^\dagger \hat{a}_{k-q}^\dagger \hat{a}_k + f_{kq} \hat{a}_k^\dagger \hat{a}_{k-q} \hat{b}_q\}, \quad (39)$$

where we exploited the translational symmetry along the waveguide axis, implying

$$\frac{1}{L} \int_0^L dz e^{-i(k-q-k')z} = \delta_{k',k-q}. \quad (40)$$

Translational symmetry results in conservation of momentum in which two photons of wave numbers k and $k - q$ scatter by emission or absorption of a phonon of wave number q . The coupling is $f_{kq} = f_{kq}^{\text{rp}} + f_{kq}^{\text{el}}$, as in Eq. (25). The coupling parameter due to radiation pressure is given by

$$f_{kq}^{\text{rp}} = -\frac{Z_q}{a_k^{\text{eff}}} \sqrt{\omega_k \omega_{k-q}} F_{kq}^{\text{rp}}, \quad (41)$$

where

$$F_{kq}^{\text{rp}} = \frac{a}{a_k^{\text{eff}}} \frac{n^2 - 1}{2} w_q^r \times \{u_k^{z*} u_{k-q}^z + u_k^{\theta*} u_{k-q}^\theta + n^2 u_k^{r*} u_{k-q}^r\}, \quad (42)$$

and all vector mode functions are evaluated on the fiber surface according to Eqs. (31). The effective radius of the photon mode a_k^{eff} is defined through $V_k^{\text{phot}} = \pi (a_k^{\text{eff}})^2 L$. In view of $\omega_q \ll \omega_k$ we approximate $\omega_{k-q} \simeq \omega_k$ in the following. The dependence of $|f_{kq}|$ on L is only through Z_q that gives $|f_{kq}| \propto 1/\sqrt{L}$.

In Figs. 6(a) and 6(b) we show the radiation pressure coupling parameter, $|f_{kq}^{\text{rp}}|/(2\pi)$, versus ka and qa for scattering that involves, respectively, the acoustic modes and the lowest vibrational modes for a fiber of length $L = 1$ cm. Radiation pressure coupling parameters have high values of about 10 kHz, in the region of $qa \approx 1.5-2$, for acoustic modes and $qa \approx 1-1.5$ for vibrational modes, which appear in the region of $ka \approx 2-3$ for photons. This region for optical photons appears at nanoscale waveguides, and the coupling is significantly decreased at microscale and larger structures.

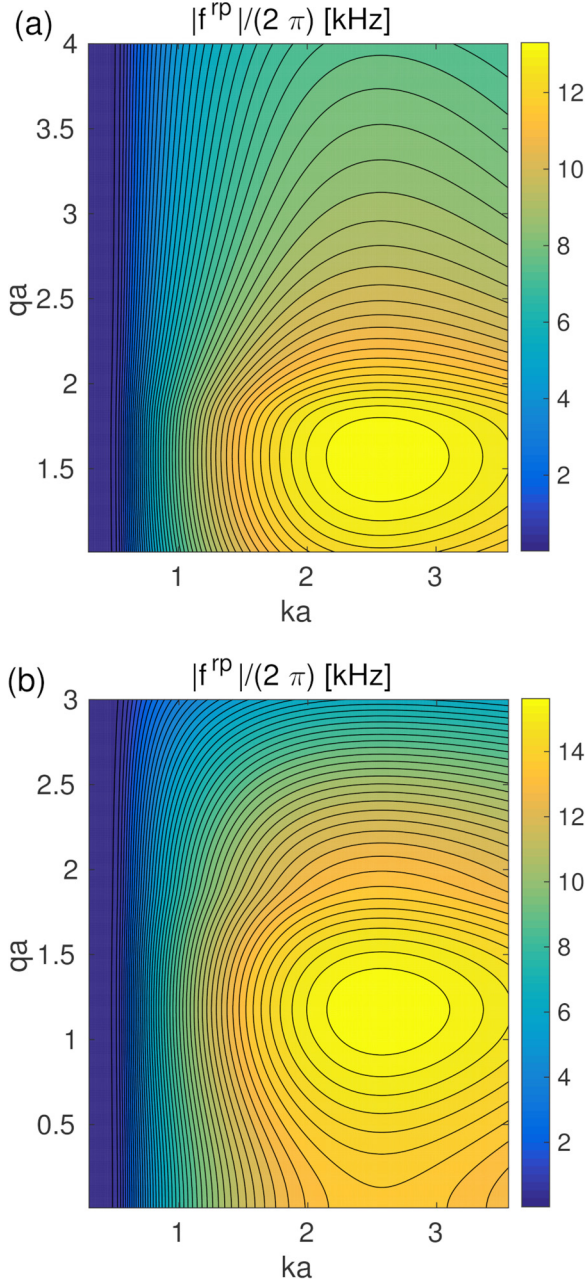


FIG. 6. The radiation pressure coupling parameter $|f_{kq}^{\text{rp}}|/(2\pi)$ contour vs. the plane $(ka - qa)$, for scattering that involves: (a) acoustic modes, and (b) vibrational modes. The fiber length is $L = 1$ cm. The optomechanical parameters f_{kq}^{rp} scale as $L^{-1/2}$.

The coupling parameter due to electrostriction is given by

$$f_{kq}^{\text{el}} = \frac{Z_q}{a_k^{\text{eff}}} \sqrt{\omega_k \omega_{k-q}} F_{kq}^{\text{el}}, \quad (43)$$

where

$$F_{kq}^{\text{el}} = \frac{\gamma_{\text{el}}}{2a_k^{\text{eff}}} \int_0^a r dr [\mathbf{u}_k^{\leq*}(r) \cdot \mathbf{u}_{k-q}^{\leq}(r)] \times \left\{ \frac{1}{r} \frac{\partial}{\partial r} [r w_q^r(r)] + i q w_q^z(r) \right\}. \quad (44)$$

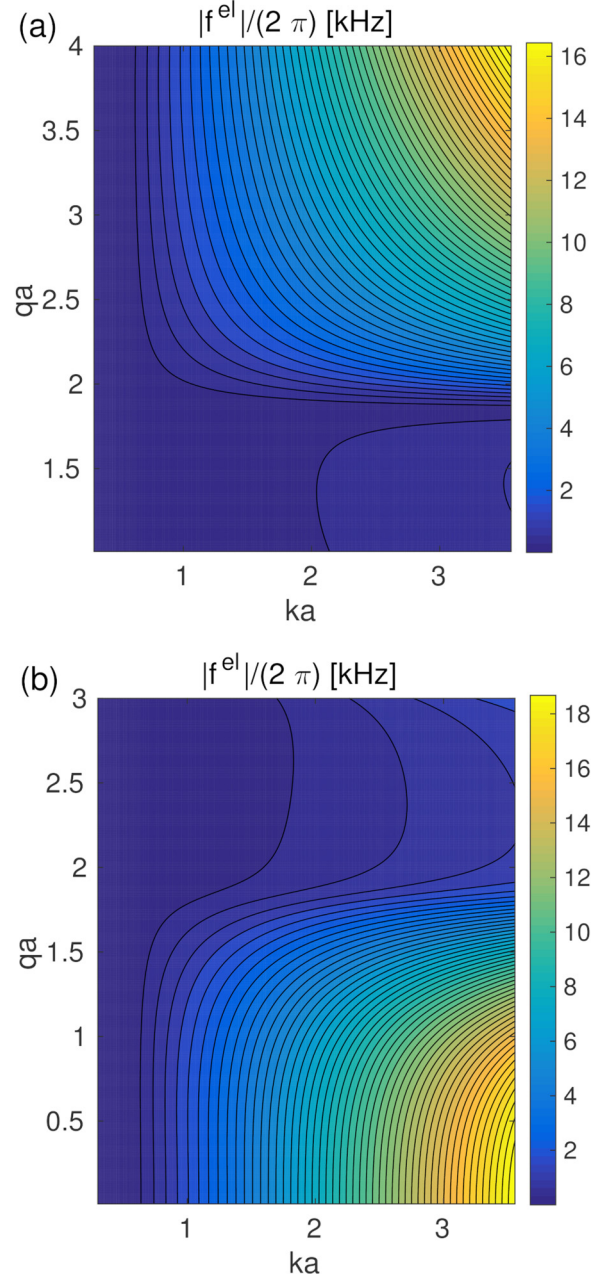


FIG. 7. The electrostriction coupling parameter $|f_{kq}^{\text{el}}|/(2\pi)$ contour vs. the plane $(ka - qa)$, for the scattering that involves: (a) acoustic modes, and (b) vibrational modes. The fiber length is $L = 1$ cm. The optomechanical parameters f_{kq}^{el} scale as $L^{-1/2}$.

In Figs. 7(a) and 7(b) we show the coupling parameter $|f_{kq}^{\text{el}}|/(2\pi)$ versus ka and qa , for scattering involving, respectively, the acoustic modes and the lowest vibrational modes again for a fiber of length $L = 1$ cm. The electrostriction parameter for dielectric materials can be written as $\gamma_{\text{el}} \approx n^4 p_{12}$, where p_{12} is the elasto-optic parameter. For silicon we have $n \approx 3.5$ and $p_{12} \approx 0.017$, hence we get $\gamma_{\text{el}} \approx 2.55$. For acoustic modes the electrostriction coupling parameters increase with increasing ka and qa , while for vibrational modes they increase with increasing ka only at small qa .

The comparison between the two coupling mechanisms show that electrostriction is small in zones where radiation

pressure is maximal, which is the case for optical light in nanoscale waveguides. But for microscale and larger waveguides electrostriction becomes dominant where radiation pressure is significantly suppressed. Nanowires of square cross sections are expected to give larger photon-phonon coupling parameters due to the fact that light is more concentrated on the boundary [9], but they have smaller mechanical quality factor relative to cylindrical nanofibers.

IV. REAL-SPACE REPRESENTATION AND BRILLOUIN GAIN PARAMETER

In this section we transform the coupled photon-phonon Hamiltonian from momentum-space to real-space representation. This is especially instructive in cases when the description can be effectively constrained to relatively narrow frequency bands, as is the case when narrowband light is injected into the nanofiber and at the same time Brillouin scattering populated only selected narrow bands of phonons. The real-space representation developed in the following provides coupled one-dimensional propagation equations for narrowband photons and phonons. As a first application we derive the Brillouin gain parameters for nanofibers measured in recent experiments from our *ab initio* calculation of the optomechanical coupling parameters f_{kq}^{rp} and f_{kq}^{el} .

A. Real-space representation

For the effectively one-dimensional photon field introduced in Sec. III A we define associated operators in real space as

$$\hat{\psi}(z) = \frac{1}{\sqrt{L}} \sum_{k \in B_{k_0}} \hat{a}_k e^{i(k-k_0)z}.$$

Here B_{k_0} denotes a suitable bandwidth of photon wave numbers centered around a central wave number k_0 . The operator $\hat{\psi}(z)$ defined such as to describe slowly varying spatial amplitudes relative to the wave e^{ik_0z} . For positive (negative) sign of k_0 the slowly varying operators $\hat{\psi}(z)$ describe right (left) propagating photons. The definition of $\hat{\psi}(z)$ implies $[\hat{\psi}(z), \hat{\psi}^\dagger(z')] = \delta(z - z')$, where the δ function is understood to be of width $\sim B_{k_0}^{-1}$. The inverse relation is

$$\hat{a}_k = \frac{1}{\sqrt{L}} \int_0^L dz \hat{\psi}(z) e^{-i(k-k_0)z}.$$

Furthermore, we approximate the photon dispersion relation shown in Fig. 2 within the relevant bandwidth B_{k_0} as $\omega_k = \omega_{k_0} + v_g(k - k_0)$, where ω_{k_0} is the bandwidth's central frequency, and $v_g = \partial\omega_k/\partial k$ is the group velocity. For the silicon nanowire considered here we have $v_g \simeq c/5$ in the range of wave numbers $1 \lesssim ka \lesssim 3$, cf. Fig. 2. In real-space representation the Hamiltonian Eq. (28) of the free photon field for modes within the bandwidth B_{k_0} is

$$\hat{H}_{\text{phot}} = \hbar\omega_{k_0} \int dz \hat{\psi}^\dagger(z) \hat{\psi}(z) - i\hbar v_g \int dz \hat{\psi}^\dagger(z) \frac{\partial \hat{\psi}(z)}{\partial z}. \quad (45)$$

In complete analogy, we define for the one-dimensional fields in Sec. III B of acoustic phonons and vibrational phonons

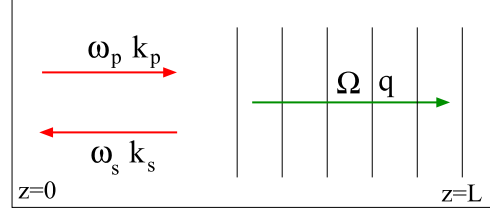


FIG. 8. The backward Stokes SBS. The pump field of frequency ω_p and wave number k_p is scattered into the Stokes field of frequency ω_s and wave number k_s , and a sound wave of frequency Ω and wave number q .

the real-space operators,

$$\hat{Q}(z) = \frac{1}{\sqrt{L}} \sum_{q \in B_{q_0}} \hat{b}_q e^{i(q-q_0)z},$$

with inverse relation,

$$\hat{b}_q = \frac{1}{\sqrt{L}} \int dz \hat{Q}(z) e^{-i(q-q_0)z}, \quad (46)$$

and commutation relation $[\hat{Q}(z), \hat{Q}^\dagger(z')] = \delta(z - z')$. The phonons have a linear dispersion with sound velocity v_s , such that within the bandwidth B_{q_0} we approximate $\Omega_q = \Omega_{q_0} + v_s(q - q_0)$. Thus, the free Hamiltonian Eq. (34) for phonons is

$$\hat{H}_{\text{phon}} = \hbar\Omega_{q_0} \int dz \hat{Q}^\dagger(z) \hat{Q}(z) - i\hbar v_s \int dz \hat{Q}^\dagger(z) \frac{\partial \hat{Q}(z)}{\partial z}. \quad (47)$$

The vibrational modes are almost dispersion-less below $qa \simeq 2$, such that $v_s \simeq 0$ in this regime.

Finally, the interaction Hamiltonian Eq. (39) is given by

$$\hat{H}_I = \sqrt{L}\hbar \int dz \times \{f^* \hat{Q}^\dagger(z) \hat{\psi}^\dagger(z) \hat{\psi}(z) + f \hat{\psi}^\dagger(z) \hat{\psi}(z) \hat{Q}(z)\}, \quad (48)$$

where f is the photon-phonon coupling parameter in the local field approximation, in which we neglect the weak dependence of f on wave numbers within the relevant bandwidths B_{q_0} and B_{k_0} of phonon and photon modes.

B. Brillouin gain parameter

The real-space description from the previous section generalizes immediately when more than one band of phonon or photon modes are considered, as we will discuss now for the case of stimulated Brillouin scattering. The result of this treatment will be a direct relation between the optomechanical coupling parameters f_{kq} and the Brillouin gain parameter, which can be observed directly in experiments. We consider the backward Brillouin scattering among two narrow band light fields, (*s*) the Stokes probe field and (*p*) the strong pump field, involving acoustic phonons, as seen in Fig. 8. We denote the central frequencies for the three bands by ω_s , ω_p , and Ω , respectively, and assume energy conservation, $\omega_p = \omega_s + \Omega$,

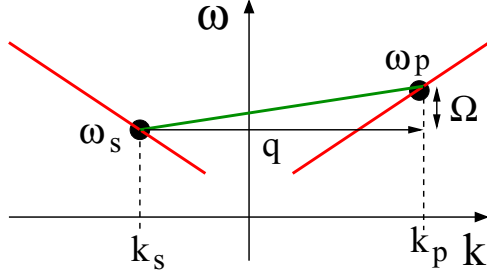


FIG. 9. The backward Stokes SBS. The process is presented schematically on the dispersion plot in order to emphasize the conservation of energy $\omega_p = \omega_s + \Omega$ and momentum $q = k_s + k_p$.

and momentum conservation, $\mathbf{k}_p = \mathbf{k}_s + \mathbf{q}$. These conditions are illustrated in Fig. 9.

Generalizing the results from the previous section to this configuration, the real-space Hamiltonian is

$$\begin{aligned} \hat{H} = & -i\hbar v_s \int dz \hat{Q}^\dagger(z) \frac{\partial \hat{Q}(z)}{\partial z} - i\hbar v_g \int dz \hat{\psi}_p^\dagger(z) \frac{\partial \hat{\psi}_p(z)}{\partial z} \\ & + i\hbar v_g \int dz \hat{\psi}_s^\dagger(z) \frac{\partial \hat{\psi}_s(z)}{\partial z} + \sqrt{L}\hbar \int dz \\ & \times \{f^* \hat{Q}^\dagger(z) \hat{\psi}_s^\dagger(z) \hat{\psi}_p(z) + f \hat{\psi}_p^\dagger(z) \hat{\psi}_s(z) \hat{Q}(z)\}, \end{aligned} \quad (49)$$

This Hamiltonian is written in an interaction picture with respect to

$$\hat{H}_0 = \hbar \int dz [\omega_p \hat{\psi}_p^\dagger(z) \hat{\psi}_p(z) + \omega_s \hat{\psi}_s^\dagger(z) \hat{\psi}_s(z) + \Omega \hat{Q}^\dagger(z) \hat{Q}(z)], \quad (50)$$

and under a rotating wave approximation where all nonresonant terms (such as $\hat{Q}^\dagger \hat{\psi}_p^\dagger \hat{\psi}_s$ or $\hat{Q}^\dagger \hat{\psi}_p^\dagger \hat{\psi}_p$) were dropped.

The equations of motion corresponding to the Hamiltonian in Eq. (49) are

$$\begin{aligned} \left(\frac{\partial}{\partial t} + v_g \frac{\partial}{\partial z} \right) \hat{\psi}_p(z,t) &= -i\sqrt{L}f \hat{Q}(z,t) \hat{\psi}_s(z,t), \\ \left(\frac{\partial}{\partial t} - v_g \frac{\partial}{\partial z} \right) \hat{\psi}_s(z,t) &= -i\sqrt{L}f^* \hat{Q}^\dagger(z,t) \hat{\psi}_p(z,t), \\ \left(\frac{\partial}{\partial t} + v_s \frac{\partial}{\partial z} \right) \hat{Q}(z,t) &= -\frac{\Gamma}{2} \hat{Q}(z,t) - i\sqrt{L}f^* \hat{\psi}_s^\dagger(z,t) \hat{\psi}_p(z,t) \\ &+ \hat{F}(z,t), \end{aligned} \quad (51)$$

where Γ is the acoustic phonon damping rate, and we neglect the photon damping. $\hat{F}(z,t)$ is the Langevin noise operator. The damping rate parameter can be extracted from the observed mechanical quality factor Q and in knowing the phonon frequency [8–13]. At steady state all time derivatives of the slowly varying operators vanish and, moreover, $\frac{\partial}{\partial z} \hat{Q}(z,t)$ can be neglected for acoustic phonons. Hence, we get

$$\hat{Q}(z,t) \approx -i \frac{2\sqrt{L}f^*}{\Gamma} \hat{\psi}_s^\dagger(z,t) \hat{\psi}_p(z,t) + \frac{2}{\Gamma} \hat{F}(z,t). \quad (52)$$

Substitutions of $\hat{Q}(z,t)$ in the equations of motion for the photon fields yields

$$\begin{aligned} \frac{\partial}{\partial z} \hat{\psi}_p(z,t) &= -\frac{2L|f|^2}{v_g \Gamma} \hat{\psi}_s^\dagger(z,t) \hat{\psi}_s(z,t) \hat{\psi}_p(z,t) \\ &- i \frac{2\sqrt{L}f}{\Gamma v_g} \hat{F}(z,t) \hat{\psi}_s(z,t), \\ \frac{\partial}{\partial z} \hat{\psi}_s(z,t) &= -\frac{2L|f^a|^2}{v_g \Gamma} \hat{\psi}_p^\dagger(z,t) \hat{\psi}_p(z,t) \hat{\psi}_s(z,t) \\ &- i \frac{2\sqrt{L}f^*}{\Gamma v_g} \hat{F}^\dagger(z,t) \hat{\psi}_p(z,t). \end{aligned} \quad (53)$$

The light field intensity is defined by [34]

$$I_p = v_g \frac{\hbar\omega}{\mathcal{A}} \langle \hat{\psi}_p^\dagger(z,t) \hat{\psi}_p(z,t) \rangle, \quad (54)$$

$$I_s = v_g \frac{\hbar\omega}{\mathcal{A}} \langle \hat{\psi}_s^\dagger(z,t) \hat{\psi}_s(z,t) \rangle, \quad (55)$$

where we set $\omega = \omega_s \simeq \omega_p$, and denote by \mathcal{A} the waveguide cross section. The strong pump field is considered as a classical field, and we use the Langevin force properties $\langle \hat{F}(z,t) \hat{\psi}_s(z,t) \rangle = \langle \hat{F}^\dagger(z,t) \hat{\psi}_s^\dagger(z,t) \rangle = 0$. Then we have

$$\frac{\partial}{\partial z} I_s = -G_B \mathcal{A} I_p I_s, \quad (56)$$

$$\frac{\partial}{\partial z} I_p = -G_B \mathcal{A} I_p I_s, \quad (57)$$

where the Brillouin gain factor is defined by

$$G_B = \frac{4L|f|^2}{\hbar\omega v_g^2 \Gamma}. \quad (58)$$

Neglecting the pump depletion, then the first of Eqs. (56) can be integrated to give $\hat{I}_s(0) = \hat{I}_s(L) \exp(G_B I_p V)$. Note that the Stokes field is propagating to the left, such that $\hat{I}_s(0)$ described the outgoing intensity. Thus, the gain parameter G_B expresses the gain in Stokes intensity per medium volume and pump intensity. We remark also that the coupling parameters in Eqs. (41) and (43) are proportional to $L^{-1/2}$, which makes $|f|^2 L$ and therefore also G_B independent of L .

We consider the scattering of the photons maximally localized in transverse direction with $ka \approx 1.74$, which is, for $a = 250$ nm, of wavelength $\lambda \simeq 900$ nm. The phonons for the backward scattering are of $qa \approx 3.48$ with the damping rate of $\Gamma/(2\pi) = 1.5$ MHz. The photon-phonon coupling parameter is $f/(2\pi) \approx 5$ kHz, for a nanowaveguide of length $L = 1$ cm. For $\Omega/(2\pi) = 15$ GHz the quality factor is $Q = 10^4$. The group velocity is about $v_g \approx c/5$. The gain efficiency is about $G_B \approx 10^4 \text{ m}^{-1} \text{ W}^{-1}$, which agrees with the experimental results in Ref. [12]. The values of all parameters used here are summarized in Table I.

The result provides a relation between the observable gain parameter G_B and the photon-phonon coupling parameter f , which agree with the one derived in Ref. [23]. The relations allow us to compare the value of the calculated photon-phonon coupling parameter to the experimental value of the gain parameter. A similar result holds for the forward Brillouin scattering involving vibrational modes.

TABLE I. Values for case study on silicon nanowire.

Name	Symbol	Value
Fiber radius	a	250 nm
Fiber length	L	1 cm
Photon group velocity	v_g	$c/5$
Photon wavelength	λ	900 nm ($ka \approx 1.74$)
Acoustic phonon frequency	$\Omega/(2\pi)$	15 GHz ($qa \approx 3.48$)
Phonon damping rate	$\Gamma/(2\pi)$	1.5 MHz
Mechanical quality factor	Q	10^4
Photon-phonon coupling	$f/(2\pi)$	5 kHz
Gain parameter	G_B	$10^4 \text{ m}^{-1}\text{W}^{-1}$

V. SUMMARY

Starting from the classical electromagnetic field Hamiltonian in dielectric media we derived the mutual coupling between light and mechanical excitations. The interaction Hamiltonian is obtained by perturbing the medium due to mechanical excitations. We treated two types of fluctuations in the dielectric medium. The first is the fluctuation in the dielectric constant that generates electrostriction coupling, and the second is fluctuations in the dielectric material boundaries that introduces radiation pressure. In order to overcome the difficulty due to the field jumps on the boundaries we expressed the Hamiltonian in terms of continuous fields. The main objective in both cases is to represent the fluctuations in terms of the mechanical displacement vector. The derived Hamiltonian can be adopted for any structure of dielectric medium ranging from nanoresonators up to bulk materials.

In quantum mechanics the electromagnetic field is represented as photons and the mechanical excitations as phonons, where the classical formulation allows direct quantization by converting the classical electric field and the displacement field into operators. We treated in much detail the case of a cylindrical nanophotonic waveguide, in which photons and phonons can propagate along the waveguide with continuum wave numbers and are strongly confined in the transverse direction with discrete modes. We explicitly solved for the photon and phonon dispersions and mode functions, where each discrete mode gives rise to photon or phonon branch. We derived the multimode photon-phonon interaction Hamiltonian for both electrostriction and radiation pressure couplings. The lowest photon branch is for HE_{11} photons, in which a single photon mode can propagate within the fiber with linear dispersion of group velocity $\sim c/5$, where for a silicon nanowire this mode is maximally localized inside the waveguide around $ka \approx 1.74$ with a small part that penetrates into the surrounding environment. The lowest phonon branch is of acoustic modes with linear dispersion, and the lowest excited phonon branch is dispersion-less of localized vibrational modes with frequency of about 10 GHz. These two phonon branches approach different linear dispersions beyond the anticrossing point.

We calculated the photon-phonon coupling parameters due to electrostriction and radiation pressure mechanisms for a silicon nanofiber. For optical light we found that radiation pressure dominates electrostriction coupling at nanoscale waveguides with coupling parameter of about 10 kHz, while electrostriction becomes dominant at larger dimensions. We

provide a tool for checking the validity of the theoretically predicted coupling parameters by relating them to the experimentally observed gain parameter. We consider Stokes backward Brillouin scattering, where a strong pump field scatters into a Stokes field and a sound wave. Starting from the real space representation of the photon and phonon Hamiltonians, we solve the field equations of motion at steady state to get the Stokes field amplification where the gain parameter is expressed in terms of the photon-phonon coupling parameter.

The results presented here provide a general outline for deriving quantum optical multimode Hamiltonians for interacting photons and phonons in optomechanical nanophotonic structures. In view of the success achieved in recent years with optomechanical structures involving single phonon and photon modes we envision that their multimode counterparts offer great possibilities to observe and exploit quantum effects in extended nanophotonic media. In particular, the optomechanical Kerr nonlinearity mediated by phonons can be exploited for the study of quantum nonlinear optics and for many-body physics of strongly correlated photons. Moreover, Brillouin induced transparency with the possibility of slow light, in analogy to EIT in cold dense atomic gases, can be achieved in the present nanoscale waveguides. The quantum optical Hamiltonian derived in the present work provides firm grounds for future explorations into these directions.

ACKNOWLEDGMENTS

We thank Raphael van Laer for useful comments. This work was funded by the European Commission (FP7-Programme) through iQUOEMS (Grant Agreement No. 323924). We acknowledge support by DFG through QUEST.

APPENDIX A: PERTURBATION THEORY OF MAXWELL'S EQUATIONS

We will show here that Eq. (2) provides the relevant part of the correction to the field Hamiltonian for a given change of the permittivity and determine the order of magnitude of the correction due to induced changes in the field amplitudes. The equations of motion following from the field Hamiltonian Eq. (1) are Maxwell's equations:

$$\nabla \times \mathbf{E} = -\mu_0 \frac{\partial \mathbf{H}}{\partial t}, \quad (\text{A1a})$$

$$\nabla \cdot (\epsilon(\mathbf{x})\mathbf{E}) = 0, \quad (\text{A1b})$$

$$\nabla \times \mathbf{H} = \epsilon(\mathbf{x}) \frac{\partial \mathbf{E}}{\partial t}, \quad (\text{A1c})$$

$$\nabla \cdot \mathbf{H} = 0, \quad (\text{A1d})$$

where \mathbf{E} and $\mathbf{H} = \mathbf{B}/\mu_0$ are the electric and magnetic fields, and $\epsilon(\mathbf{x})$ is the (dimensionless) permittivity of the assumed dielectric, lossless, and nonmagnetic material. Maxwell's equations imply for the magnetic field

$$\frac{1}{c^2} \frac{\partial^2 \mathbf{H}}{\partial t^2} + \nabla \times \left(\frac{\epsilon_0}{\epsilon(\mathbf{x})} \nabla \times \mathbf{H} \right) = 0.$$

Harmonic solutions $\mathbf{H}(\mathbf{x}, t) = \mathbf{H}_k(\mathbf{x})e^{-i\omega_k t}$ therefore fulfill the eigenvalue equation,

$$\nabla \times \left(\frac{\epsilon_0}{\epsilon(\mathbf{x})} \nabla \times \mathbf{H}_k \right) = \frac{\omega_k^2}{c^2} \mathbf{H}_k. \quad (\text{A2})$$

The operator on the left-hand side is Hermitian [37] and, therefore, the eigenmodes are orthonormal, $\int_V dV \mathbf{H}_k^*(\mathbf{x}) \mathbf{H}_l(\mathbf{x}) = \delta_{kl}$. When the permittivity is changed slightly $\epsilon(\mathbf{x}) \rightarrow \epsilon(\mathbf{x}) + \delta\epsilon(\mathbf{x})$ the perturbed eigenmodes $\mathbf{H}_k + \delta\mathbf{H}_k$ will remain orthonormal, which implies for the first-order corrections,

$$\int_V dV \{ \delta\mathbf{H}_k^*(\mathbf{x}) \mathbf{H}_l(\mathbf{x}) + \mathbf{H}_k^*(\mathbf{x}) \delta\mathbf{H}_l(\mathbf{x}) \} = 0. \quad (\text{A3})$$

On the other hand, the electric displacement field $\mathbf{D} = \epsilon(\mathbf{x})\mathbf{E}$ corresponding to field mode \mathbf{H}_k is $\mathbf{D}_k = i\omega_k^{-1} \nabla \times \mathbf{H}_k$ due to Eq. (A1c), and the same relation holds for the first-order perturbation $\delta\mathbf{D}_k = i\omega_k^{-1} \nabla \times \delta\mathbf{H}_k$. Note that this statement does not apply in the same way to the electric field $\mathbf{E}_k = i[\epsilon(\mathbf{x})\omega_k]^{-1} \nabla \times \mathbf{H}_k$ whose perturbation contains, apart from $\delta\mathbf{H}_k$, further contributions proportional to $\delta\epsilon(\mathbf{x})$. For a general electric displacement field $\mathbf{D}(\mathbf{x}, t) = \sum_k \mathbf{D}_k(\mathbf{x}) d_k(t)$ with amplitudes $d_k(t)$, one therefore finds

$$\begin{aligned} & \int_V dV \frac{1}{\epsilon(\mathbf{x})} \delta\mathbf{D}^* \mathbf{D} \\ &= \sum_{k,l} \frac{d_k^* d_l}{\omega_k \omega_l} \int_V dV \frac{1}{\epsilon(\mathbf{x})} (\nabla \times \delta\mathbf{H}_k^*) (\nabla \times \mathbf{H}_l) \\ &= \frac{1}{\epsilon_0} \sum_{k,l} \frac{d_k^* d_l}{\omega_k \omega_l} \int_V dV \delta\mathbf{H}_k^* \nabla \times \left(\frac{\epsilon_0}{\epsilon(\mathbf{x})} \nabla \times \mathbf{H}_l \right) \\ &= \frac{1}{\epsilon_0} \sum_{k,l} \frac{d_k^* d_l}{c^2} \frac{\omega_k}{\omega_l} \int_V dV \delta\mathbf{H}_k^* \mathbf{H}_l, \end{aligned}$$

where we used the eigenvalue Eq. (A2) in the last step. Overall, this implies

$$\begin{aligned} & \int_V dV \frac{1}{\epsilon(\mathbf{x})} (\delta\mathbf{D}^* \mathbf{D} + \mathbf{D}^* \delta\mathbf{D}) \\ &= \frac{1}{\epsilon_0} \sum_{k,l} \frac{d_k^* d_l}{c^2} \int_V dV \left(\frac{\omega_k}{\omega_l} \delta\mathbf{H}_k^* \mathbf{H}_l + \frac{\omega_l}{\omega_k} \mathbf{H}_k^* \delta\mathbf{H}_l \right) \simeq 0, \end{aligned}$$

where we used Eq. (A3) and the fact that the optical photon frequency is not changed appreciably in Brillouin scattering, that is $\omega_k/\omega_l = 1 + \mathcal{O}(\omega_{\text{phonon}}/\omega_{\text{photon}})$. Thus, the contribution to the perturbation of the field Hamiltonian due to the corrections in the field amplitudes, $\int_V dV \epsilon(\mathbf{x})^{-1} \delta|\mathbf{D}|^2$, is at most of magnitude $\mathcal{O}(\omega_{\text{phonon}}/\omega_{\text{photon}})$ to first order in $\delta\epsilon$ (or equivalently, in the mechanical displacement \mathbf{Q}). Note that this is not the case for $\int_V dV \epsilon(\mathbf{x}) \delta|\mathbf{E}|^2$ for the reason given above. The reasoning presented here also shows that the first-order correction of the Hamiltonian due to the perturbation of the magnetic field amplitudes vanishes exactly due to Eq. (A3).

APPENDIX B: NANOFIBER ELECTROMAGNETIC FIELD

Here we present the rigorous derivation of the nanofiber modes [35,38] for a cylindrical waveguide. We start from the Maxwell's Eq. (A1a) in cylindrical coordinates (r, θ, z) . The fields E_θ , H_θ , E_r , and H_r can be expressed in terms of the

axial fields E_z and H_z by

$$\begin{aligned} E_r &= -i \frac{\beta}{\mu_0 \epsilon \omega^2 - \beta^2} \left(\frac{\partial}{\partial r} E_z + \frac{\mu_0 \omega}{\beta} \frac{1}{r} \frac{\partial}{\partial \theta} H_z \right), \\ E_\theta &= -i \frac{\beta}{\mu_0 \epsilon \omega^2 - \beta^2} \left(\frac{1}{r} \frac{\partial}{\partial \theta} E_z - \frac{\mu_0 \omega}{\beta} \frac{\partial}{\partial r} H_z \right), \\ H_r &= -i \frac{\beta}{\mu_0 \epsilon \omega^2 - \beta^2} \left(\frac{\partial}{\partial r} H_z - \frac{\mu_0 \omega}{\beta} \frac{1}{r} \frac{\partial}{\partial \theta} E_z \right), \\ H_\theta &= -i \frac{\beta}{\mu_0 \epsilon \omega^2 - \beta^2} \left(\frac{1}{r} \frac{\partial}{\partial \theta} H_z + \frac{\mu_0 \omega}{\beta} \frac{\partial}{\partial r} E_z \right), \end{aligned} \quad (\text{B1})$$

where β is the axial wave number. The solution for the axial fields is given by

$$\begin{aligned} E_z(\mathbf{x}, t) &= R(r) e^{\pm i l \theta} e^{-i(\beta z - \omega t)}, \\ H_z(\mathbf{x}, t) &= R(r) e^{\pm i l \theta} e^{-i(\beta z - \omega t)}, \end{aligned} \quad (\text{B2})$$

where $l = 0, 1, 2, \dots$. The radial function $R(r)$ obeys the Bessel equation

$$\left[\frac{1}{r} \frac{\partial}{\partial r} + \frac{\partial^2}{\partial r^2} + \left(k^2 - \beta^2 - \frac{l^2}{r^2} \right) \right] R(r) = 0, \quad (\text{B3})$$

where $k^2 = \mu_0 \epsilon \omega^2$. The solution inside the fiber, that is $r < a$, with $\epsilon = \epsilon_0 n^2$, is given by

$$\begin{aligned} E_z(r, \theta, z, t) &= A J_l(pr) e^{-i(\beta z - \omega t \pm l \theta)}, \\ H_z(r, \theta, z, t) &= B J_l(pr) e^{-i(\beta z - \omega t \pm l \theta)}, \end{aligned} \quad (\text{B4})$$

where $p = \sqrt{n^2 k_0^2 - \beta^2}$, with $k_0 = \omega/c$ is the free-space wave number. The solution on the outside of the fiber, that is $(r > a)$, with $\epsilon = \epsilon_0$, is given by

$$\begin{aligned} E_z(r, \theta, z, t) &= C K_l(qr) e^{-i(\beta z - \omega t \pm l \theta)}, \\ H_z(r, \theta, z, t) &= D K_l(qr) e^{-i(\beta z - \omega t \pm l \theta)}, \end{aligned} \quad (\text{B5})$$

where $q = \sqrt{\beta^2 - k_0^2}$.

Using the relations Eq. (B1), the solutions inside the fiber, that is $r < a$, are given by

$$\begin{aligned} E_r(r, \theta, z, t) &= \left\{ -i \frac{\beta}{p} A J_l'(pr) + \frac{\mu_0 \omega}{p} (\pm l) B \frac{J_l(pr)}{pr} \right\} \\ & \quad e^{i(\omega t - \beta z \pm l \theta)}, \\ E_\theta(r, \theta, z, t) &= \left\{ \frac{\beta}{p} (\pm l) A \frac{J_l(pr)}{pr} + i \frac{\mu_0 \omega}{p} B J_l'(pr) \right\} \\ & \quad e^{i(\omega t - \beta z \pm l \theta)}, \end{aligned} \quad (\text{B6})$$

$$E_z(r, \theta, z, t) = A J_l(pr) e^{i(\omega t - \beta z \pm l \theta)},$$

and

$$\begin{aligned} H_r(r, \theta, z, t) &= \left\{ -i \frac{\beta}{p} B J_l'(pr) - \frac{\epsilon \omega}{p} (\pm l) A \frac{J_l(pr)}{pr} \right\} \\ & \quad e^{i(\omega t - \beta z \pm l \theta)}, \\ H_\theta(r, \theta, z, t) &= \left\{ \frac{\beta}{p} (\pm l) B \frac{J_l(pr)}{pr} - i \frac{\epsilon \omega}{p} A J_l'(pr) \right\} \\ & \quad e^{i(\omega t - \beta z \pm l \theta)}, \end{aligned} \quad (\text{B7})$$

$$H_z(r, \theta, z, t) = B J_l(pr) e^{i(\omega t - \beta z \pm l \theta)}.$$

The solutions outside of the fiber, that is $r > a$, are given by

$$\begin{aligned}
 E_r(r, \theta, z, t) &= \left\{ i \frac{\beta}{q} C K_l'(qr) - \frac{\mu_0 \omega}{q} (\pm l) D \frac{K_l(qr)}{qr} \right\} \\
 &\quad e^{i(\omega t - \beta z \pm l \theta)}, \\
 E_\theta(r, \theta, z, t) &= \left\{ -\frac{\beta}{q} (\pm l) C \frac{K_l(qr)}{qr} - i \frac{\mu_0 \omega}{q} D K_l'(qr) \right\} \\
 &\quad e^{i(\omega t - \beta z \pm l \theta)}, \\
 E_z(r, \theta, z, t) &= C K_l(qr) e^{i(\omega t - \beta z \pm l \theta)},
 \end{aligned} \tag{B8}$$

and

$$\begin{aligned}
 H_r(r, \theta, z, t) &= \left\{ i \frac{\beta}{q} D K_l'(qr) + \frac{\epsilon_0 \omega}{q} (\pm l) C \frac{K_l(qr)}{qr} \right\} \\
 &\quad e^{i(\omega t - \beta z \pm l \theta)}, \\
 H_\theta(r, \theta, z, t) &= \left\{ -\frac{\beta}{q} (\pm l) D \frac{K_l(qr)}{qr} + i \frac{\epsilon_0 \omega}{q} C K_l'(qr) \right\} \\
 &\quad e^{i(\omega t - \beta z \pm l \theta)}, \\
 H_z(r, \theta, z, t) &= D K_l(qr) e^{i(\omega t - \beta z \pm l \theta)}.
 \end{aligned} \tag{B9}$$

The plus sign (+ l) refers to the right-handed solution of the transverse field, and the minus sign ($-l$) refers to the left-handed solution. The linearly polarized solution can be composed as a superposition of right- and left-handed solutions.

The constants A , B , C , and D can be fixed by the boundary condition between the inside and outside fields on the fiber surface, where the fields E_z , E_θ , H_z , and H_θ are continuous on the boundary. For the constants we obtain the relations

$$\begin{aligned}
 C &= A \frac{J_l(pa)}{K_l(qa)}, \quad D = CB/A, \\
 B &= A \frac{i\beta(\pm l)}{\mu_0 \omega} \left[\frac{1}{(pa)^2} + \frac{1}{(qa)^2} \right] \\
 &\quad \times \left(\frac{J_l'(pa)}{pa J_l(pa)} + \frac{K_l'(qa)}{qa K_l(qa)} \right)^{-1}, \tag{B10}
 \end{aligned}$$

and A can be fixed by the normalization condition. The continuity leads to a characteristic equation that determines the wave number β . For the EH modes, in which E_z is larger than H_z , we get

$$\begin{aligned}
 \frac{J_{l-1}(pa)}{pa J_l(pa)} &= \left(\frac{1+n^2}{2n^2} \right) \frac{K_{l-1}(qa) + K_{l+1}(qa)}{2qa K_l(qa)} + \frac{l}{p^2 a^2} \\
 &\quad + \left\{ \left(\frac{n^2-1}{2n^2} \right)^2 \left(\frac{K_{l-1}(qa) + K_{l+1}(qa)}{2qa K_l(qa)} \right)^2 \right. \\
 &\quad \left. + \left(\frac{l\beta}{nk_0} \right)^2 \left(\frac{1}{q^2 a^2} + \frac{1}{p^2 a^2} \right)^2 \right\}^{1/2}, \tag{B11}
 \end{aligned}$$

and for the HE modes, in which E_z is smaller than H_z , we get

$$\begin{aligned}
 \frac{J_{l-1}(pa)}{pa J_l(pa)} &= \left(\frac{1+n^2}{2n^2} \right) \frac{K_{l-1}(qa) + K_{l+1}(qa)}{2qa K_l(qa)} + \frac{l}{p^2 a^2} \\
 &\quad - \left\{ \left(\frac{n^2-1}{2n^2} \right)^2 \left(\frac{K_{l-1}(qa) + K_{l+1}(qa)}{2qa K_l(qa)} \right)^2 \right. \\
 &\quad \left. + \left(\frac{l\beta}{nk_0} \right)^2 \left(\frac{1}{q^2 a^2} + \frac{1}{p^2 a^2} \right)^2 \right\}^{1/2}. \tag{B12}
 \end{aligned}$$

The equations can be solved numerically or graphically and give a set of discrete solutions for β at each l that are specified by index m . The modes are labeled by HE_{lm} and EH_{lm} . The transverse modes EH_{0m} are usually denoted by TM_{0m} , where H_z vanishes. The transverse modes HE_{0m} are usually denoted by TE_{0m} , where E_z vanishes. The modes HE_{lm} and EH_{lm} are termed hybrid modes, as all field components are nonzero. The hybrid modes represent screw rays and l is associated with the orbital angular momentum along the fiber axis.

APPENDIX C: NANOFIBER MECHANICAL VIBRATIONS

We present the elastic waves in a cylindrical waveguide of isotropic medium [36]. The displacement vector is given by $\mathbf{Q} = (Q_r, Q_\theta, Q_z)$. In the theory of elasticity the displacement can be derived directly from the scalar ϕ and vector $\vec{\Psi}$ potentials. In general, we can make the decomposition $\mathbf{Q} = \mathbf{Q}_l + \mathbf{Q}_t$, where $\mathbf{Q}_l = \nabla \phi$ is a divergence-free vector, and $\mathbf{Q}_t = \nabla \times \vec{\Psi}$ is an irrotational vector. Hence, the material displacements are obtained from the potentials by

$$\mathbf{Q} = \nabla \phi + \nabla \times \vec{\Psi}. \tag{C1}$$

The scalar field obeys the wave equation

$$\nabla^2 \phi - \frac{1}{v_l^2} \frac{\partial^2 \phi}{\partial t^2} = 0, \tag{C2}$$

where v_l is the velocity of the longitudinal wave, in which $\nabla \times \mathbf{Q}_l = 0$. The vector potential obeys the wave equation

$$\nabla^2 \vec{\Psi} - \frac{1}{v_t^2} \frac{\partial^2 \vec{\Psi}}{\partial t^2} = 0, \tag{C3}$$

where v_t is the velocity of the transverse wave, in which $\nabla \cdot \mathbf{Q}_t = 0$. As the three displacements are expressed in terms of four scalar potentials, one needs an extra relation between the potentials. The constraint condition usually used is $\nabla \cdot \vec{\Psi} = 0$, but the $\nabla \cdot \vec{\Psi} \neq 0$ condition is also possible. The two displacement parts propagate independently. The longitudinal component, \mathbf{Q}_l , propagates with velocity v_l , and the transverse component, \mathbf{Q}_t , propagates with velocity v_t .

Now we concentrate in the solution of the wave equations in cylindrical coordinates. For harmonic waves of frequency Ω , we have

$$\begin{aligned}
 \phi(r, \theta, z, t) &= \phi(r, \theta, z) e^{-i\Omega t}, \\
 \Psi_i(r, \theta, z, t) &= \Psi_i(r, \theta, z) e^{-i\Omega t}, \tag{C4}
 \end{aligned}$$

with $(i = r, \theta, z)$. The Laplacian of scalar and vector potentials are defined by

$$\begin{aligned} \nabla^2 \phi &= \nabla \cdot \nabla \phi, \\ \nabla^2 \vec{\Psi} &= \nabla(\nabla \cdot \vec{\Psi}) - \nabla \times \nabla \times \vec{\Psi}. \end{aligned} \quad (C5)$$

The wave equations are given explicitly by

$$\begin{aligned} \nabla^2 \phi + \frac{\Omega^2}{v_t^2} \phi &= 0, \\ \nabla^2 \Psi_r - \frac{1}{r^2} \Psi_r - \frac{2}{r^2} \frac{\partial \Psi_\theta}{\partial \theta} + \frac{\Omega^2}{v_t^2} \Psi_r &= 0, \\ \nabla^2 \Psi_\theta - \frac{1}{r^2} \Psi_\theta + \frac{2}{r^2} \frac{\partial \Psi_r}{\partial \theta} + \frac{\Omega^2}{v_t^2} \Psi_\theta &= 0, \\ \nabla^2 \Psi_z + \frac{\Omega^2}{v_t^2} \Psi_z &= 0. \end{aligned} \quad (C6)$$

The equations for ϕ and Ψ_z are separated, and for Ψ_r and Ψ_θ are coupled. The Laplacian ∇^2 is given in cylindrical coordinates. The solution for ϕ has the form

$$\phi(r, \theta, z, t) = R(r)\Theta(\theta)e^{i(qz - \Omega t)}, \quad (C7)$$

where $R(r)$ and $\Theta(\theta)$ obey the equations

$$\begin{aligned} \frac{\partial^2 \Theta}{\partial \theta^2} + n^2 \Theta &= 0, \\ \frac{\partial^2 R}{\partial r^2} + \frac{1}{r} \frac{\partial R}{\partial r} + \left(\frac{\Omega^2}{v_t^2} - q^2 \right) R - \frac{n^2}{r^2} R &= 0, \end{aligned} \quad (C8)$$

with $(n = 0, 1, 2, \dots)$. The general solution has the form

$$\phi(r, \theta, z, t) = A J_n(\eta_t r) \cos(n\theta) e^{i(qz - \Omega t)}, \quad (C9)$$

with $\eta_t^2 = \frac{\Omega^2}{v_t^2} - q^2$. The solution for Θ can be either $\cos(n\theta)$ or $\sin(n\theta)$, and for $R(r)$ the solution is the Bessel functions of the first kind. Similar solution holds for Ψ_z , where

$$\Psi_z(r, \theta, z, t) = B J_n(\eta_t r) \cos(n\theta) e^{i(qz - \Omega t)}, \quad (C10)$$

with $\eta_t^2 = \frac{\Omega^2}{v_t^2} - q^2$.

The solutions for Ψ_r and Ψ_θ have the form

$$\begin{aligned} \Psi_r(r, \theta, z, t) &= \bar{\Psi}_r(r) \sin(n\theta) e^{i(qz - \Omega t)}, \\ \Psi_\theta(r, \theta, z, t) &= \bar{\Psi}_\theta(r) \cos(n\theta) e^{i(qz - \Omega t)}, \end{aligned} \quad (C11)$$

where

$$\begin{aligned} \bar{\Psi}_r(r) &= D J_{n-1}(\eta_t r) + C J_{n+1}(\eta_t r), \\ \bar{\Psi}_\theta(r) &= D J_{n-1}(\eta_t r) - C J_{n+1}(\eta_t r). \end{aligned} \quad (C12)$$

Here using $\cos(n\theta)$ in Ψ_r implies $\sin(n\theta)$ in Ψ_θ , and viceversa.

We have four constants A, B, C , and D . We still are free to add another relation between the potentials. But the usually used relation of $\nabla \cdot \vec{\Psi} = 0$ gives a complex relation. Here we use the simple relation $\Psi_r = -\Psi_\theta$, which leads to $D = 0$.

The general solutions can be given by

$$\begin{aligned} \phi(r, \theta, z, t) &= A J_n(\eta_t r) \cos(n\theta) e^{i(qz - \Omega t)}, \\ \Psi_r(r, \theta, z, t) &= C J_{n+1}(\eta_t r) \sin(n\theta) e^{i(qz - \Omega t)}, \\ \Psi_\theta(r, \theta, z, t) &= -C J_{n+1}(\eta_t r) \cos(n\theta) e^{i(qz - \Omega t)}, \\ \Psi_z(r, \theta, z, t) &= B J_n(\eta_t r) \sin(n\theta) e^{i(qz - \Omega t)}. \end{aligned} \quad (C13)$$

The constants A, B , and C are fixed from boundary conditions.

The displacement components are given in terms of the potentials by

$$\begin{aligned} Q_r &= \frac{\partial \phi}{\partial r} + \frac{1}{r} \frac{\partial \Psi_z}{\partial \theta} - \frac{\partial \Psi_\theta}{\partial z}, \\ Q_\theta &= \frac{1}{r} \frac{\partial \phi}{\partial \theta} - \frac{\partial \Psi_z}{\partial r} + \frac{\partial \Psi_r}{\partial z}, \\ Q_z &= \frac{\partial \phi}{\partial z} - \frac{1}{r} \frac{\partial \Psi_r}{\partial \theta} + \frac{1}{r} \frac{\partial (r \Psi_\theta)}{\partial r}. \end{aligned} \quad (C14)$$

The boundary condition implies the surface, at $r = a$, to be free, which leads to the equation that relates Ω, q , and n . Three cases can be treated, which are (i) torsional waves for $n = 0$, where Q_θ is independent of θ , (ii) longitudinal waves for $n = 0$ where Q_r and Q_z are independent of θ , and (iii) flexural waves for $n = 1$ where Q_r, Q_θ , and Q_z are dependent on (r, θ, z) .

1. Torsional waves

For axially symmetric torsional waves with $n = 0$, which are the simplest case for elastic waves in a rod, the displacement along the θ direction is defined by

$$Q_\theta(r, z, t) = -\frac{\partial}{\partial r} \Psi_z, \quad (C15)$$

and $Q_r = Q_z = 0$, where the potentials ϕ, Ψ_r , and Ψ_θ are taken to be zero. Here the solution for the potential is $\Psi_z = \Psi_z(r, z, t)$ and has the form

$$\Psi_z = B J_0(\eta_t r) e^{i(qz - \Omega t)}, \quad (C16)$$

where B is an amplitude and $\eta_t^2 = \frac{\Omega^2}{v_t^2} - q^2$. The displacement reads

$$Q_\theta(r, z, t) = B \eta_t J_1(\eta_t r) e^{i(qz - \Omega t)}. \quad (C17)$$

The force-free surface leads to the condition [36] $\eta_t a J_2(\eta_t a) = 0$, where either $\eta_t a = 0$ or $J_2(\eta_t a) = 0$. The case of $\eta_t a = 0$ gives the solution

$$\Psi_z \approx -B \frac{r^2 \eta_t^2}{6} e^{i(q_0 z - \Omega t)}, \quad (C18)$$

with $q_0 = \Omega/v_t$. Hence, we have

$$Q_\theta^0 \approx \frac{1}{3} B \eta_t^2 r e^{i(q_0 z - \Omega t)}. \quad (C19)$$

The condition $J_2(\eta_t a) = 0$ gives a set of roots, e.g., $\varepsilon_1 = 5.136, \varepsilon_2 = 8.417, \varepsilon_3 = 11.620, \dots$, and we write $\varepsilon_n = \eta_t a$, where we can write the solutions as

$$Q_\theta^n = B \frac{\varepsilon_n}{a} J_1(\varepsilon_n r/a) e^{i(q_n z - \Omega t)}, \quad (C20)$$

with $q^2 = \frac{\Omega^2}{v_t^2} - \frac{\varepsilon_n^2}{a^2}$.

2. Longitudinal modes

For longitudinal acoustic modes with $n = 0$ from symmetry consideration we have $Q_r = Q_r(r, z, t)$, $Q_z = Q_z(r, z, t)$, and $Q_\theta = 0$. Here we have $\Psi_r = \Psi_z = 0$, and hence the displacements are related to the potentials by

$$\begin{aligned} Q_r &= \frac{\partial \phi}{\partial r} - \frac{\partial \Psi_\theta}{\partial z}, \\ Q_z &= \frac{\partial \phi}{\partial z} + \frac{1}{r} \frac{\partial(r\Psi_\theta)}{\partial r}. \end{aligned} \quad (\text{C21})$$

The solutions for the potentials are

$$\begin{aligned} \phi &= A J_0(\eta_l r) e^{i(qz - \Omega t)}, \\ \Psi_\theta &= -C J_1(\eta_l r) e^{i(qz - \Omega t)}, \end{aligned} \quad (\text{C22})$$

where $\eta_i^2 = \frac{\Omega^2}{v_i^2} - q^2$, for $(i = l, t)$. The requirement of the stress to vanish on the fiber boundary, ($r = a$), leads to the

Pochhammer frequency equation,

$$(q^2 - \eta_l^2)^2 \frac{\eta_l a J_0(\eta_l a)}{J_1(\eta_l a)} + 4q^2 \eta_t^2 \frac{\eta_t a J_0(\eta_t a)}{J_1(\eta_t a)} = 2\eta_l^2 (q^2 + \eta_t^2). \quad (\text{C23})$$

In the limit of $qa \ll 1$ one gets the sound wave linear dispersion $\Omega \approx v_l q$. The displacements are given explicitly by

$$\begin{aligned} Q_r &= -\{A\eta_l J_1(\eta_l r) - iqC J_1(\eta_t r)\} e^{i(qz - \Omega t)}, \\ Q_\theta &= 0, \\ Q_z &= \{iqA J_0(\eta_l r) - \eta_t C J_0(\eta_t r)\} e^{i(qz - \Omega t)}. \end{aligned} \quad (\text{C24})$$

From boundary condition we can get also relations between A and C . Namely, the vanishing of the stress and the strain on the surface yields [36]

$$2iq\eta_l J_1(\eta_l a)A = [\eta_t^2 - q^2] J_1(\eta_t a)C. \quad (\text{C25})$$

-
- [1] M. Aspelmeyer, S. Gröblacher, K. Hammerer, and N. Kiesel, *J. Opt. Soc. Am. B* **27**, A189 (2010).
- [2] M. Aspelmeyer, T. J. Kippenberg, and F. Marquardt, *Rev. Mod. Phys.* **86**, 1391 (2014).
- [3] M. Aspelmeyer, T. J. Kippenberg, and F. Marquardt, in *Cavity Optomechanics: Nano- and Micromechanical Resonators Interacting with Light*, edited by M. Aspelmeyer, T. J. Kippenberg, and F. Marquardt (Springer, Heidelberg, 2014), pp. 1–4.
- [4] W. B. Bowen and G. J. Milburn, *Quantum Optomechanics* (CRC Press, Boca Raton, FL, 2016).
- [5] K. Hammerer, C. Genes, D. Vitali, P. Tombesi, G. Milburn, C. Simon, and D. Bouwmeester, in *Cavity Optomechanics: Nano- and Micromechanical Resonators Interacting with Light*, edited by M. Aspelmeyer, T. J. Kippenberg, and F. Marquardt (Springer, Heidelberg, 2014), pp. 25–56.
- [6] M. Eichenfield, J. Chan, R. M. Camacho, K. J. Vahala, and O. Painter, *Nature* **462**, 78 (2009).
- [7] A. H. Safavi-Naeini and O. Painter, in *Cavity Optomechanics: Nano- and Micromechanical Resonators Interacting with Light*, edited by M. Aspelmeyer, T. J. Kippenberg, and F. Marquardt (Springer, Heidelberg, 2014), pp. 195–231.
- [8] R. Van Laer, B. Kuyken, D. Van Thourhout, and R. Baets, *Opt. Photon. News* **26**, 51 (2015), issue December.
- [9] P. T. Rakich, C. Reinke, R. Camacho, P. Davids, and Z. Wang, *Phys. Rev. X* **2**, 011008 (2012).
- [10] H. Shin, W. Qiu, R. Jarecki, J. A. Cox, R. H. Olsson III, A. Starbuck, Z. Wang, and P. T. Rakich, *Nature Commun.* **4**, 1944 (2013).
- [11] R. Van Laer, B. Kuyken, D. Van Thourhout, and R. Baets, *Nature Photon.* **9**, 199 (2015).
- [12] R. Van Laer, A. Bazin, B. Kuyken, R. Baets, and D. Van Thourhout, *New J. Phys.* **17**, 115005 (2015).
- [13] E. A. Kittlaus, H. Shin, and P. T. Rakich, *Nature Photonics* **10**, 463 (2016).
- [14] L. Thevenaz, *Nat. Photon.* **2**, 474 (2008).
- [15] A. Kobayakov, M. Sauer, and D. Chowdhury, *Adv. Opt. Photon.* **2**, 1 (2010).
- [16] B. J. Eggleton, C. G. Poulton, and R. Pant, *Adv. Opt. Photon.* **5**, 536 (2013).
- [17] G. Bahl and T. Carmon, in *Cavity Optomechanics: Nano- and Micromechanical Resonators Interacting with Light*, edited by M. Aspelmeyer, T. J. Kippenberg, and F. Marquardt (Springer, Heidelberg, 2014), pp. 157–168.
- [18] I. L. Fabelinskii, *Molecular Scattering of Light* (Plenum, New York, 1968).
- [19] R. W. Boyd, *Nonlinear Optics* (Elsevier, Amsterdam, 2008), 3rd ed.
- [20] C. Wolff, M. J. Steel, B. J. Eggleton, and C. G. Poulton, *Phys. Rev. A* **92**, 013836 (2015).
- [21] G. S. Agarwal and S. S. Jha, *Phys. Rev. A* **88**, 013815 (2013).
- [22] S. G. Johnson, M. Ibanescu, M. A. Skorobogatiy, O. Weisberg, J. D. Joannopoulos, and Y. Fink, *Phys. Rev. E* **65**, 066611 (2002).
- [23] R. Van Laer, R. Baets, and D. Van Thourhout, *Phys. Rev. A* **93**, 053828 (2016).
- [24] J. E. Sipe and M. J. Steel, *New J. Phys.* **18**, 045004 (2016).
- [25] R. Pant, C. G. Poulton, D.-Y. Choi, H. Mcfarlane, S. Hile, E. Li, L. Thevenaz, B. Luther-Davies, S. J. Madden, and B. J. Eggleton, *Opt. Express* **19**, 8285 (2011).
- [26] E. Vetsch, D. Reitz, G. Sagué, R. Schmidt, S. T. Dawkins, and A. Rauschenbeutel, *Phys. Rev. Lett.* **104**, 203603 (2010).
- [27] A. Goban, K. S. Choi, D. J. Alton, D. Ding, C. Lacroûte, M. Pototschnig, T. Thiele, N. P. Stern, and H. J. Kimble, *Phys. Rev. Lett.* **109**, 033603 (2012).
- [28] C. Wuttke, G. D. Cole, and A. Rauschenbeutel, *Phys. Rev. A* **88**, 061801 (2013).
- [29] R. J. Glauber and M. Lewenstein, *Phys. Rev. A* **43**, 467 (1991).
- [30] W. Qiu, P. T. Rakich, H. Shin, H. Dong, M. Soljacic, and Z. Wang, *Opt. Express* **21**, 31402 (2013).
- [31] T. Gruner and D. G. Welsch, *Phys. Rev. A* **53**, 1818 (1996).
- [32] J. E. Sipe, N. A. R. Bhat, P. Chak, and S. Pereira, *Phys. Rev. E* **69**, 016604 (2004).

- [33] P. D. Drummond and M. Hillery, *The Quantum Theory of Nonlinear Optics* (Cambridge University Press, Cambridge, UK, 2014).
- [34] R. Loudon, *The Quantum Theory of Light* (Oxford University Press, Oxford, UK, 2000), 3rd ed.
- [35] F. L. Kien, J. Liang, K. Hakuta, and V. Balykin, [Optics Commun.](#) **242**, 445 (2004).
- [36] J. D. Achenbach, *Wave Propagation in Elastic Solids* (North-Holland Publishing Company, Amsterdam, 1973).
- [37] M. Skorobogatiy and J. Yang, in *Fundamentals of Photonic Crystal Guiding* (Cambridge University Press, Cambridge, UK, 2009).
- [38] J. D. Jackson, *Classical Electrodynamics* (John Wiley and Sons, New York, USA, 1999), 3rd ed.